JLAB-THY-98-17

Quantum Monte Carlo Studies of Relativistic Effects in Light Nuclei

J. L. Forest*, V. R. Pandharipande†
Department of Physics, University of Illinois at Urbana-Champaign, 1110 W. Green Street, Urbana, IL 61801

A. Arriaga‡
Centro de Fisica Nuclear da Universidade de Lisboa, Avenida Gama Pinto 2, 1699 Lisboa, Portugal

(May 14, 1998)

Abstract

Relativistic Hamiltonians are defined as the sum of relativistic one-body kinetic energy, two- and three-body potentials and their boost corrections. In this work we use the variational Monte Carlo method to study two kinds of relativistic effects in the binding energy of ^{3}H and ^{4}He. The first is due to the nonlocalities in the relativistic kinetic energy and relativistic one-pion exchange potential (OPEP), and the second is from boost interaction. The OPEP contribution is reduced by $\sim 15\%$ by the relativistic nonlocality, which may also have significant effects on pion exchange currents. However, almost all of this reduction is canceled by changes in the kinetic energy and other interaction terms, and the total effect of the nonlocalities on the binding energy is very small. The boost interactions, on the other hand, give repulsive contributions of ~ 0.4 (1.9) MeV in ^{3}H (^{4}He) and account for $\sim 37\%$ of the phenomenological part of the three-nucleon interaction needed in the nonrelativistic Hamiltonians.

PACS numbers: 21.45.+v, 21.60.Ka, 24.10.Jv

I. INTRODUCTION

It is generally accepted that QCD is the fundamental theory of strong interactions, however, due to quark confinement, the genuine QCD degrees of freedom are not explicit at low energies. In low energy nuclear physics, nucleons and mesons are believed to be the physical (effective) degrees of freedom. In the nonrelativistic many-body theory, nuclei are regarded as bound states of nucleons interacting via two- and three-body potentials. All the sub-nucleonic and meson degrees of freedom, as well as relativistic effects are, in some way, absorbed in these potentials. Typically the nonrelativistic Hamiltonian is expressed as

$$H_{NR} = \sum_i \frac{p_i^2}{2m_i} + \sum_{i<j} v_{ij} + \sum_{i<j<k} V_{ijk} + \cdots, \tag{1.1}$$

and models of two- and three-body potentials are constructed by fitting observed data. The ellipsis in Eq. (1.1) represents N-body interactions ($N \geq 4$) which are thought to be much smaller than two- or three-nucleon interactions, and therefore neglected.

The central problem is to solve the many-body Schrödinger equation:

$$H_{NR}\,|\Psi\rangle = E|\Psi\rangle. \tag{1.2}$$

The eigenvalues E can be compared with experimental energies, and the eigenstates $|\Psi\rangle$ can be used both to study the nuclear structure and probe it through electron-nucleus scattering experiments, and to calculate rates of nuclear reactions which may have important applications in several domains of physics.

Schrödinger equation (1.2) is difficult to solve due to the large spin and isospin dependence of v_{ij} and V_{ijk}. Several techniques have been developed, among which are Faddeev-Yakubovsky [1], Harmonic-Hyperspherical basis [2], and Quantum Monte Carlo (QMC) [3,4] methods. The first two methods are limited to solving 3- and 4-nucleon systems, whereas with the third method it is now possible to calculate the ground state energy and wave function for A=2–8 nuclei with great accuracy.

Some of the results obtained by Pudliner *et al.* [5] are listed in Table I. The Argonne v_{18} 2-body potential [6], fitted to NN scattering data and the deuteron binding energy,

and Urbana IX 3-body potential [5] constrained to give the correct binding energy of ^{3}H and density of nuclear matter, are used in these calculations. It works rather well for ^{4}He, however, as can be seen from Table I, the A=6, 7 and 8 nuclei appear to be systematically underbound. It is interesting to note that a large fraction of the total v_{ij} comes from the one-pion exchange potential (OPEP) and the dominant part of V_{ijk} comes from two-pion exchange. Also notice that the three-body interaction is much smaller than the two-body interaction, yet it is crucial to obtain the observed energies, because of the large cancelation between the kinetic energy and the two-body potential energy.

Although the nonrelativistic QMC techniques have advanced to such a level that the binding energies of light nuclei predicted by a realistic Hamiltonian can be calculated with <1% error [3,5], the effective description of nuclear dynamics by means of nonrelativistic Hamiltonians may have intrinsic deficiencies. In particular, when the nonrelativistic potentials are fit to the experimental data, relativistic effects are automatically buried in these potentials. How well can these effects be represented by means of local nonrelativistic potentials is an important question to be answered. In other words, we may investigate whether an explicit and more correct treatment of relativistic effects can resolve the systematic underbinding of the nonrelativistic results for $A = 6, 7, 8$ nuclei.

Furthermore, with the recently completed multi GeV electron accelerator facilities such as TJNAF, experiments will be performed at energy and momentum transfer regimes where relativistic effects are substantial. Clearly, investigation of these effects has become increasingly important. Above all, no matter how small the relativistic effects might be, understanding them is a fundamental quest, just like understanding the fine and hyperfine structures in the hydrogen atom.

Several approaches have been developed to study various aspects of the relativistic effects in few-body nuclear physics. They can be classified in two main categories: effective field theories and relativistic Hamiltonian dynamics. Within the first one, the Bethe-Salpeter equations for the two- and three-body systems have been solved using a separable kernel [7]. Also covariant three-dimensional reductions of the relativistic integral equations have been

applied, along with one-boson exchange models for the kernels, to the three-nucleon system. Here we refer to minimal relativity in the Blankenbecler-Sugar equations [8] and, more recently, to the spectator (Gross) equations [9]. In the relativistic Hamiltonian dynamics approach, relativistic covariance is achieved through the Poincaré group theory. One application of this method is the light front dynamics, which has been applied to the two-body system [10], and the other is the instant form.

The present interest in the relativistic Hamiltonian dynamics in the instant form stems from the fact that the ground states of the Hamiltonian can be studied with the Quantum Monte Carlo methods that have already been developed in the nonrelativistic approach. Earlier [11,12] and the present study are limited to the A=2, 3 and 4 nuclei, but attempts to study larger nuclei are in progress. In addition, the use of short-range phenomenological terms in the interaction gives the flexibility to allow a very good fit to the two-body scattering data with $\chi^2 \sim 1$. And finally, it is not obvious that the entire short and intermediate range 2-nucleon interaction can be represented as due to the exchange of a few types of mesons. Thus more general ways of studying relativistic effects in nuclei are desirable.

In this paper we report new results for the binding energies of the $A = 3, 4$ systems, using the relativistic Hamiltonian dynamics in the instant form, where for the first time the nonlocalities induced by the relativistic effects in the one-pion-exchange potential (OPEP) are taken into account. In Sec. II we discuss the relativistic Hamiltonian used in this work. In Sec. III we apply Variational Monte Carlo (VMC) techniques and present results. Finally we summarize in Sec. IV. Some of the detailed derivations involved in this work are given in the Appendix.

II. THE RELATIVISTIC HAMILTONIAN

In relativistic Hamiltonian dynamics in instant form the momentum (**P**) and angular momentum (**J**) generators are chosen in the conventional way and therefore are independent of interaction, while the Hamiltonian (H) and boost (**K**) generators have interaction terms.

Based on the pioneering work of Bakamjian and Thomas [13] and Foldy [14], the relativistic Hamiltonian can be expressed as:

$$H_R = \sum_i \left(\sqrt{m_i^2 + p_i^2} - m_i\right) + \sum_{i<j} [\tilde{v}_{ij} + \delta v_{ij}(\mathbf{P}_{ij})] + \sum_{i<j<k} \left[\tilde{V}_{ijk} + \delta V_{ijk}(\mathbf{P}_{ijk})\right] + \cdots, \quad (2.1)$$

where $\tilde{v}_{ij}$ are two-body potentials in the "rest frame" of particles i and j (i.e. the frame in which $\mathbf{P}_{ij} = \mathbf{p}_i + \mathbf{p}_j = 0$). Similarly $\tilde{V}_{ijk}$ is the three-body potential in the frame in which $\mathbf{P}_{ijk} = \mathbf{p}_i + \mathbf{p}_j + \mathbf{p}_k = 0$. The $\delta v_{ij}(\mathbf{P}_{ij})$ and $\delta V_{ijk}(\mathbf{P}_{ijk})$ are called "boost interactions" and depend upon the total momentum of the interacting particles. Obviously, $\delta v_{ij}(\mathbf{P}_{ij}=0)$ and $\delta V_{ijk}(\mathbf{P}_{ijk}=0)$ vanish. The H_{NR} contains approximations to the kinetic energy T, $\tilde{v}_{ij}$ and $\tilde{V}_{ijk}$, and totally neglects the boost interactions. In the case of deuteron, we can always go to its center of mass (c.m.) frame where total momentum $\mathbf{P}_{ij}=0$. The $\tilde{v}_{ij}$ is adequate to describe the deuteron in its "rest frame", however, in $A > 2$ nuclei the total momentum of any pair of nucleons is not necessarily zero in the c.m. of the whole nucleus, therefore the interaction between the pair can not be correctly described by $\tilde{v}_{ij}$ alone.

Two kinds of relativistic effects in the interaction are studied in this work: the boost interaction $\delta v_{ij}(\mathbf{P}_{ij})$ due to the motion of the c.m. of nucleons i and j in the rest frame of the whole nucleus, and the nonlocality due to the relative motion of two nucleons in their own c.m. frame. The latter will affect the "rest frame" potential $\tilde{v}_{ij}$. The boost interaction has been studied in detail in Refs. [17,11,12], so we will only give a brief discussion. On the other hand, the treatment of the nonlocality of OPEP in quantum Monte Carlo calculations is discussed in detail.

The boost interaction $\delta v(\mathbf{P}_{ij})$ is determined from the "rest frame" potential $\tilde{v}_{ij}$ through relativistic covariance [15,16]. The $\delta v(\mathbf{P}_{ij})$ is expanded in powers of $P_{ij}^2/4m^2$ and only the leading corrections are considered in this work. The $\delta v(\mathbf{P}_{ij})$ is given by:

$$\delta v(\mathbf{P}) = -\frac{P^2}{8m^2}\tilde{v} + \frac{i}{8m^2}\left[\,\mathbf{P}\cdot\mathbf{r}\mathbf{P}\cdot\mathbf{p}, \tilde{v}\,\right] + \frac{i}{8m^2}\left[\,(\boldsymbol{\sigma}_1 - \boldsymbol{\sigma}_2)\times\mathbf{P}\cdot\mathbf{p}, \tilde{v}\,\right], \quad (2.2)$$

where the subscripts ij of $\tilde{v}$, $\mathbf{P}$, $\mathbf{p}$ and $\mathbf{r}$ have been suppressed for brevity. Here $\mathbf{p}=(\mathbf{p}_i - \mathbf{p}_j)/2$ is the relative momentum operator, and $\boldsymbol{\sigma}=2\mathbf{s}$ are the Pauli matrices for spin 1/2 particles.

Various aspects of $\delta v(\mathbf{P})$ are discussed in Ref. [17]. The first two terms of Eq. (2.2) are denoted as δv_{RE} and δv_{LC}; they have simple classical origins in the relativistic energy-momentum relation and Lorentz contraction. The last term contains contributions from Thomas precession and quantum effects. They are denoted as δv_{TP} and δv_{QM} and are much smaller than the first two terms. For example, the contributions of δv_{RE}, δv_{LC}, δv_{TP} and δv_{QM} to the energy of triton are found [11] to be 0.23(2), 0.10(1), 0.016(2) and -0.004(2) MeV, respectively. Since the main contribution comes from the first two terms, for simplicity, we neglected the last two terms in the 3-, 4-body calculations in this work.

In addition to the boost interaction, another source of relativistic effects comes from the nonlocality. In the following discussion we will use the two-nucleon c.m. frame in which boost interaction vanishes, and focus on the two-body "rest frame" interaction. In most existing nonrelativistic potential models, the OPEP has been calculated using the nonrelativistic Pauli spinors. Without πNN form factors, it is given in momentum space by:

$$\tilde{v}_{\pi,NR}(\mathbf{q}) = -\frac{f_{\pi NN}^2}{\mu^2}\,\frac{\boldsymbol{\sigma}_i\cdot\mathbf{q}\boldsymbol{\sigma}_j\cdot\mathbf{q}\boldsymbol{\tau}_i\cdot\boldsymbol{\tau}_j}{\mu^2+q^2}, \tag{2.3}$$

where $f_{\pi NN}$ is the pion–nucleon coupling constant, μ is the pion mass and $\mathbf{q}$ is the momentum transfer,

$$\mathbf{q} = \mathbf{p} - \mathbf{p}'. \tag{2.4}$$

Here $\mathbf{p}$ and $\mathbf{p}'$ are the initial and final momenta of nucleon i in the center of mass frame, and the $\tilde{v}_{\pi,NR}$ is local, i.e. it depends only on $\mathbf{q}$.

In contrast if one uses relativistic Dirac spinors the on-shell OPEP has the form:

$$\tilde{v}_{\pi,Rel}(\mathbf{p}',\mathbf{p}) = \frac{m}{\sqrt{m^2+p'^2}}\,\tilde{v}_{\pi,NR}(\mathbf{q})\,\frac{m}{\sqrt{m^2+p^2}}. \tag{2.5}$$

This potential is dependent not only on $\mathbf{q}$ but also on $\mathbf{p}$ and $\mathbf{p}'$, which results in a nonlocal potential in the configuration space. The interaction (2.5) is regarded as energy independent and used in many-body Schrödinger equations. By expanding the square roots it can be easily verified that the leading correction $(\tilde{v}_{\pi,Rel} - \tilde{v}_{\pi,NR})$ is of order p^2/m^2, i.e., of order v^2/c^2 where v denotes the velocity of the nucleons in the center of mass frame.

In Ref. [17] it is shown that the relation between the boost interaction $\delta v(\mathbf{P})$ and the static $\tilde{v}_{NR}$ is independent of the origin of $\tilde{v}_{NR}$ up to order P^2/m^2, and presumably beyond. Thus the knowledge of the static $\tilde{v}_{NR}$ is sufficient to obtain $\delta v(\mathbf{P})$. In contrast the above relation between $\tilde{v}_{\pi,Rel}$ and $\tilde{v}_{\pi,NR}$ (Eq. 2.5) is specific for the interaction due to exchange of pseudoscalar mesons by Dirac nucleons via either pseudoscalar or pseudovector coupling. By expanding the square roots in Eq. (2.5) we obtain:

$$\tilde{v}_{\pi,Rel}(\mathbf{p}',\mathbf{p}) = \tilde{v}_{\pi,NR}(\mathbf{q})\left(1 - \frac{p'^2}{2m^2} - \frac{p^2}{2m^2} + \cdots\right), \tag{2.6}$$

whereas the interactions generated by exchange of scalar (S) or vector (V) mesons have different relations [17]:

$$\tilde{v}_{S,Rel}(\mathbf{p}',\mathbf{p}) = \tilde{v}_{S,NR}(\mathbf{q})\left(1 - \frac{(\mathbf{p}'+\mathbf{p})^2}{2m^2} + \cdots\right), \tag{2.7}$$

$$\tilde{v}_{V,Rel}(\mathbf{p}',\mathbf{p}) = \tilde{v}_{V,NR}(\mathbf{q})\left(1 + \frac{(\mathbf{p}'+\mathbf{p})^2}{2m^2} + \cdots\right). \tag{2.8}$$

Realistic models of nuclear forces contain momentum dependent terms which presumably take into account some of the relativistic corrections to the phenomenological short and intermediate range parts of $\tilde{v}_{NN}$. However, most configuration space models do not contain long range, momentum dependent tensor forces occuring in $\tilde{v}_{\pi,Rel}$. In exact calculations the tensor force can not be generally expanded in powers of p^2/m^2. In any truncated expansion the force diverges at large values of p, and can yield divergent attraction.

In the present work the two-nucleon potential is expressed as:

$$\tilde{v}_{NN} = \tilde{v}_{\pi,Rel} + \tilde{v}_R \tag{2.9}$$

where $\tilde{v}_R$ is the remaining part of the 2-body potential which is phenomenological. We can also write the OPEP given in Eq. (2.5) as:

$$\tilde{v}_{\pi,Rel} = \tilde{v}_{\pi,NR} + (\tilde{v}_{\pi,Rel} - \tilde{v}_{\pi,NR}). \tag{2.10}$$

The term in parenthesis is the relativistic correction. The nonrelativistic potential models do not consider this correction explicitly: the data is fit using $\tilde{v}_{\pi,NR}$ in Eq. (2.9), thus some

of its effects go into the phenomenological part of the potential $\tilde{v}_R$. The $\tilde{v}_R$ in relativistic Hamiltonian differs from that in nonrelativistic Hamiltonian due to the difference in $\tilde{v}_{\pi,Rel}$ and $\tilde{v}_{\pi,NR}$ as well as that in the kinetic energy operators.

We construct our H_R to be phase equivalent to the isoscalar part of the nonrelativistic H_{NR} containing Argonne v_{18}. The relativistic effects can then be studied by comparing results obtained from our H_R and the isoscalar H_{NR} without considering the small isospin symmetry breaking terms in the latter. The relativistic Hamiltonian for two-nucleon system in its center of mass frame is chosen as:

$$H_R = 2\sqrt{p^2+m^2} - 2m \; + \; \frac{m}{\sqrt{m^2+p'^2}}\,\tilde{v}_{\pi,NR}(\mathbf{q})\,\frac{m}{\sqrt{m^2+p^2}} \; + \; \tilde{v}_R. \tag{2.11}$$

where $\tilde{v}_R$ has the same form as the isoscalar part of Argonne v_{18} [6]:

$$\tilde{v}_R = \sum_{p=1,14} v_p(r_{ij}) O^p_{ij}, \tag{2.12}$$

$$O^{p=1,14}_{ij} = 1, \boldsymbol{\tau}_i\cdot\boldsymbol{\tau}_j, \boldsymbol{\sigma}_i\cdot\boldsymbol{\sigma}_j, (\boldsymbol{\sigma}_i\cdot\boldsymbol{\sigma}_j)(\boldsymbol{\tau}_i\cdot\boldsymbol{\tau}_j), S_{ij}, S_{ij}(\boldsymbol{\tau}_i\cdot\boldsymbol{\tau}_j), \mathbf{L}\cdot\mathbf{S}, \mathbf{L}\cdot\mathbf{S}(\boldsymbol{\tau}_i\cdot\boldsymbol{\tau}_j),$$
$$L^2, L^2(\boldsymbol{\tau}_i\cdot\boldsymbol{\tau}_j), L^2(\boldsymbol{\sigma}_i\cdot\boldsymbol{\sigma}_j), L^2(\boldsymbol{\sigma}_i\cdot\boldsymbol{\sigma}_j)(\boldsymbol{\tau}_i\cdot\boldsymbol{\tau}_j), (\mathbf{L}\cdot\mathbf{S})^2, (\mathbf{L}\cdot\mathbf{S})^2(\boldsymbol{\tau}_i\cdot\boldsymbol{\tau}_j). \tag{2.13}$$

The $\tilde{v}_{\pi,NR}$ used in Argonne v_{18} is given by:

$$\tilde{v}_{\pi,NR}(\mathbf{r}) = \frac{1}{3}\mu\frac{f^2_{\pi NN}}{4\pi}\left[Y_\pi(r)\boldsymbol{\sigma}_i\cdot\boldsymbol{\sigma}_j + T_\pi(r)S_{ij}\right]\boldsymbol{\tau}_i\cdot\boldsymbol{\tau}_j, \tag{2.14}$$

where

$$Y_\pi(r) = \frac{e^{-\mu r}}{\mu r}\left(1-e^{-cr^2}\right), \tag{2.15}$$

$$T_\pi(r) = \left(1+\frac{3}{\mu r}+\frac{3}{(\mu r)^2}\right)\left(1-e^{-cr^2}\right)^2, \tag{2.16}$$

$$S_{ij} = 3\boldsymbol{\sigma}_i\cdot\hat{r}\boldsymbol{\sigma}_j\cdot\hat{r} - \boldsymbol{\sigma}_i\cdot\boldsymbol{\sigma}_j. \tag{2.17}$$

We note that this $\tilde{v}_{\pi,NR}$ does not contain the part of $\boldsymbol{\sigma}_i\cdot\boldsymbol{\sigma}_j\boldsymbol{\tau}_i\cdot\boldsymbol{\tau}_j$ interaction which acquires a $\delta(r_{ij})$ function form in the limit of point particles. This $\delta-$function is probably spread out by the finite size of the nucleons, and contributes to the short range part of v_{NN}. However, it is difficult to extract it from the phenomenological models. Moreover the dominant contribution and the nonlocality effect seem to come from the tensor part of OPEP.

Recently, after completion of the present work, Kamada and Glöckle [18] found an elegant method to obtain a potential v_{Rel} that gives exactly the same phase shifts with relativistic kinetic energy that a known v_{NR} gives with nonrelativistic kinetic energy. Our objective here is not just to find a v_{Rel} that is phase equivalent to the Argonne v_{18}; we additionally require it to have the $\tilde{v}_{\pi,Rel}$ long range behavior. Both relativistic and nonrelativistic models of $\tilde{v}$ contain theoretical long range OPEP; the scattering data is used to determine only the phenomenological part $\tilde{v}_R$ in these interactions. Our two models are not as exactly phase equivalent as Kamada and Glöckle's v_{Rel} and v_{NR} are, however the differences in their phase shifts are negligibly small compared to the uncertainties in the Nijmegen phase shifts [19].

The parameters of the function $v_p(r_{ij})$ of $\tilde{v}_R$ are obtained by fitting the phase shifts and deuteron binding energy. Traditionally phase shifts are calculated in configuration space, however, in the relativistic case, the Hamiltonian contains $\sqrt{m^2-\nabla^2}$ which is nonlocal in configuration space, therefore we calculate them in momentum space. The details of the momentum-space technique have been discussed in Ref. [20].

Some of the important phase shifts are plotted in Fig. 1. The diamond symbols represent the reference nonrelativistic phase shifts obtained with H_{NR}, the plus symbols represent those calculated from H_R before re-adjusting the parameters in $v_p(r)$, and the square symbols correspond to those after. The reference phase shifts are almost exactly reproduced by the relativistic Hamiltonian H_R as indicated by the good overlap of the diamond and square symbols in Fig. 1. The deviations between the plus and diamond symbols reflect the total effect of replacing nonrelativistic kinetic energy and $\tilde{v}_{\pi,NR}$ by the relativistic kinetic energy and $\tilde{v}_{\pi,Rel}$ in H_{NR}, and are not too large except for the mixing parameter E_1 of ${}^3S_1 - {}^3D_1$. This indicates that relativistic nonlocal effects in two nucleon scattering at $E_{\rm lab} < 400$ MeV are rather small. E_1 is primarily determined by the tensor force; the relatively large change in E_1 is due to the nonlocality of the tensor force in $\tilde{v}_{\pi,Rel}$.

The new two-body potential is essentially phase equivalent to isoscalar part of Argonne v_{18} and predicts similar deuteron properties as listed in Table II. Note that the present H_{NR} and H_R do not contain electromagnetic interactions. The experimental value of deuteron

binding energy (-2.224 MeV) can be obtained from the full Argonne v_{18} with electromagnetic interactions. The 14 operator components of the relativistic and nonrelativistic potentials are compared in Fig. 2. Only the static part of the relativistic OPEP, obtained by setting $m/\sqrt{p^2+m^2}$ equal to unity is used in Fig. 2. Since it is the same as the nonrelativistic OPEP, the difference between the potentials shown in the figure is entirely due to that in the phenomenological part $\tilde{v}_R$. Equation (2.5) shows that the $\tilde{v}_{\pi,Rel}$ is smaller than the $\tilde{v}_{\pi,NR}$ for p or $p' \neq 0$.

The deuteron S- and D-wave functions are shown in Fig. 3. Here the relativistic D-wave is slightly smaller than the nonrelativistic one, presumably because the relativistic tensor potential is smaller than the nonrelativistic tensor potential (Eq. 2.5) for large p and p'. The deuteron wave functions in momentum space are shown in Fig. 4. Note that the relativistic wave functions are not very different from the nonrelativistic ones. The ratio of the two momentum space D-wave functions can be easily understood as discussed below.

The exact ground state wave function Ψ can be expanded in a complete set of states $|i\rangle$:

$$|\Psi\rangle = \sum_i \phi_i |i\rangle. \tag{2.18}$$

For a Hamiltonian given by $T+v$, where $|i\rangle$ are eigenstates of T, the amplitudes ϕ_i are given by

$$\phi_i = -\frac{\langle i|v|\Psi\rangle}{\langle i|T-E_0|i\rangle}, \tag{2.19}$$

as can be verified from the Schrödinger equation $H|\Psi\rangle = E_0|\Psi\rangle$. Here E_0 is the ground state energy,

In the case of the deuteron we can choose T as the kinetic energy operator and $|i\rangle$ as S- and D-waves with momentum p, denoted by $|p_l\rangle$, for $l = S, D$. The amplitudes $\phi_l(p)$ of these waves give the deuteron wave function in momentum space. We can estimate the difference between the nonrelativistic and relativistic deuteron D-state wave function at large momentum by assuming that it is primarily generated by the OPEP. In the nonrelativistic case this gives:

$$\phi_{D,NR}(p) = -\frac{m}{p^2}\langle p_D|\tilde{v}_{\pi,NR}|\Psi\rangle, \tag{2.20}$$

where we have neglected the E_0 in the denominator of Eq. (2.19), since it is much smaller than the kinetic energy p^2/m at large p. In the relativistic case

$$\phi_{D,Rel}(p) = -\frac{1}{2(\sqrt{m^2+p^2}-m)}\frac{m}{\sqrt{m^2+p^2}}\langle p_D|\tilde{v}_{\pi,NR}|\Psi\rangle, \tag{2.21}$$

where the first factor is the relativistic kinetic energy denominator, and the second comes from the m/E' factor in the $\tilde{v}_{\pi,Rel}$ (Eq. 2.5). The other m/E factor in the $\tilde{v}_{\pi,Rel}$ operates on the Ψ. It is set to unity because most of the deuteron wave function has small relative momenta.

Neglecting the small difference between the relativistic and nonrelativistic Ψ, the ratio of the $\phi_D(p)$ is found to be

$$\frac{\phi_{D,Rel}(p)}{\phi_{D,NR}(p)} = \frac{p^2}{2(\sqrt{m^2+p^2}-m)\sqrt{m^2+p^2}}. \tag{2.22}$$

The above estimate is fairly close to the ratio of the calculated D-wave functions as can be seen in Fig. 5. Note that this ratio is smaller if the $\tilde{v}_{\pi,Rel}$ is used with the nonrelativistic kinetic energy in $\phi_{D,Rel}(p)$ (dotted line), and it is larger than one when the $\tilde{v}_{\pi,NR}$ is used with the relativistic kinetic energy (dot-dashed line). The relativistic corrections to the interaction and kinetic energies have opposite effects on the wave function. The difference between the S-wave functions is influenced by the changes in the kinetic energy and the $\tilde{v}_R$. The effects of these changes on the phase shifts and the deuteron energy must cancel by construction, and they seem to largely cancel in the $\phi_S(p)$.

Some of the deuteron momentum space results are listed in Table III. This table offers a microscopic view of how various relativistic effects were buried in the nonrelativistic models. Relativistic nonlocalities reduce the OPEP contribution by ~2.6 MeV, while the relativistic kinetic energy is smaller by ~ -1 MeV, giving a net effect of 1.6 MeV which is canceled by the change in the phenomenological $\tilde{v}_R$.

The variational Monte Carlo calculations for the $A > 2$ systems have to be carried out

in configuration space. We therefore have to Fourier transform the $\tilde{v}_{\pi,Rel}$ which depends on both $\mathbf{p}$ and $\mathbf{p}'$ (Eq. 2.5), yielding a nonlocal potential in configuration space:

$$\tilde{v}_{\pi,Rel}(\mathbf{r}',\mathbf{r}) = \int \frac{\mathrm{d}^3p}{(2\pi)^3}\frac{\mathrm{d}^3p'}{(2\pi)^3}\, \mathrm{e}^{-\mathrm{i}\mathbf{p}'\cdot\mathbf{r}'}\, \tilde{v}_{\pi,Rel}(\mathbf{p}',\mathbf{p})\, \mathrm{e}^{\mathrm{i}\mathbf{p}\cdot\mathbf{r}}. \tag{2.23}$$

The exact integral in Eq. (2.23) is extremely difficult to calculate. The series obtained by expanding $\tilde{v}_{\pi,Rel}(\mathbf{p}',\mathbf{p})$ in powers of p^2/m^2 is given by:

$$\tilde{v}_{\pi,Rel}(\mathbf{p}',\mathbf{p}) = \tilde{v}_{\pi,NR}(\mathbf{q})\left(1 - \frac{p^2+p'^2}{2m^2} + \frac{3p^4+2p^2p'^2+3p'^4}{8m^4} + \cdots\right) \tag{2.24}$$

However, this series does not have good convergence. In the case of deuteron, the expectation value of $\tilde{v}_{\pi,NR}$, for the eigenfunction of our relativistic Hamiltonian is -21.39 MeV. The term in $\tilde{v}_{\pi,Rel}$, of order $1/m^2$, contributes 3.48 MeV to the $\langle\tilde{v}_{\pi,Rel}\rangle$, while that of order $1/m^4$ gives -1.45 MeV, and the exact $\langle\tilde{v}_{\pi,Rel} - \tilde{v}_{\pi,NR}\rangle$ is 2.59 MeV. Therefore the series converges slowly to the exact value. This may appear surprising because the expectation value of the kinetic energy of the deuteron (Table III) is only about 20 MeV, giving $p^2/m^2 \approx 0.02$ on average. However, the deuteron has large momentum components via the D-wave, or equivalently the tensor correlations, and most of the OPEP contribution is from those. Thus it is not surprising that the expectation value of OPEP is sensitive to higher powers of nucleon velocities.

For the relativistic OPEP, a good convergence is achieved by using the variables:

$$\mathbf{Q} = \frac{1}{2}(\mathbf{p}+\mathbf{p}'), \qquad \mathbf{q} = \mathbf{p}-\mathbf{p}', \tag{2.25}$$

$$\mathbf{x} = \frac{1}{2}(\mathbf{r}+\mathbf{r}'), \qquad \mathbf{y} = \mathbf{r}-\mathbf{r}', \tag{2.26}$$

for which

$$\begin{aligned}\tilde{v}_{\pi,Rel} &= \tilde{v}_{\pi,NR}(\mathbf{q})\frac{m^2}{\sqrt{(m^2+Q^2+q^2/4)^2-(\mathbf{Q}\cdot\mathbf{q})^2}},\\ &= \tilde{v}_{\pi,NR}(\mathbf{q})\left[1 - \frac{Q^2+\frac{q^2}{4}}{m^2+Q^2+\frac{q^2}{4}} + \frac{1}{2}\frac{m^2(\mathbf{Q}\cdot\mathbf{q})^2}{\left(m^2+Q^2+\frac{q^2}{4}\right)^3} + \cdots\right].\end{aligned} \tag{2.27}$$

Here we expanded the $\tilde{v}_{\pi,Rel}$ in powers of $(\mathbf{Q}\cdot\mathbf{q})^2/(m^2+Q^2+q^2/4)^2$. This series appears to converge rapidly. In the case of deuteron, the leading relativistic correction given by

the second term is 2.7 MeV, the third term gives -0.18 MeV, and the exact value is 2.59 MeV. The third term contains θ_{Qq} dependence and results in complicated operator forms as shown in the Appendix. Moreover, the third and higher terms account for only ~ 4 % of the relativistic correction to OPEP expectation value in the deuteron (*i.e.* ~ 0.6 % of $\langle\tilde{v}_{\pi,Rel}\rangle$). Therefore only the first two terms are considered in this work, and the relativistic OPEP is approximated by:

$$\tilde{v}_{\pi,Rel} = \frac{m^2}{m^2+Q^2+\frac{q^2}{4}}\,\tilde{v}_{\pi,NR}(\mathbf{q}). \tag{2.28}$$

With this $\tilde{v}_{\pi,Rel}$ in Eq. (2.9), we refit the phase shifts and deuteron binding energy. The parameters in $v_p(r)$ are very similar to those obtained with the exact $\tilde{v}_{\pi,Rel}$ given by Eq. (2.5). The new phase shifts and the relativistic potentials are very similar to those shown in Figs. 1 and 2.

The configuration space potential (Eq. 2.23) is given by:

$$\tilde{v}_{\pi,Rel}(\mathbf{x},\mathbf{y}) = \int \frac{\mathrm{d}^3Q}{(2\pi)^3}\frac{\mathrm{d}^3q}{(2\pi)^3}\,\frac{m^2}{m^2+Q^2+\frac{q^2}{4}}\,\tilde{v}_{\pi,NR}(\mathbf{q})\,\mathrm{e}^{\mathrm{i}(\mathbf{Q}\cdot\mathbf{y}+\mathbf{q}\cdot\mathbf{x})}, \tag{2.29}$$

and is simple to evaluate. The $\tilde{v}_{\pi,NR}$ (Eq. 2.14) in momentum space is given by:

$$\begin{aligned}\tilde{v}_{\pi,NR}(\mathbf{q}) &= \int \tilde{v}_{\pi,NR}(\mathbf{r})\, e^{i\mathbf{q}\cdot\mathbf{r}}\,\mathrm{d}^3r,\\ &= \frac{1}{3}\mu f_{\pi NN}^2\left[\mathcal{Y}_\pi(q)\,\boldsymbol{\sigma}_i\cdot\boldsymbol{\sigma}_j + \mathcal{T}_\pi(q)\left(\boldsymbol{\sigma}_i\cdot\boldsymbol{\sigma}_j - \frac{3}{q^2}\boldsymbol{\sigma}_i\cdot\mathbf{q}\boldsymbol{\sigma}_j\cdot\mathbf{q}\right)\right]\boldsymbol{\tau}_i\cdot\boldsymbol{\tau}_j,\end{aligned} \tag{2.30}$$

where

$$\mathcal{Y}_\pi(q) = \int Y_\pi(r) j_0(qr) r^2 \mathrm{d}r, \tag{2.31}$$

$$\mathcal{T}_\pi(q) = \int T_\pi(r) j_2(qr) r^2 \mathrm{d}r. \tag{2.32}$$

Substituting these into Eq. (2.29) gives:

$$\tilde{v}_{\pi,Rel}(x,y) = \frac{1}{3}\mu\frac{f_{\pi NN}^2}{4\pi}\, f(y)\,\left[F_{\sigma\tau}(x,y)\,\boldsymbol{\sigma}_i\cdot\boldsymbol{\sigma}_j + F_{t\tau}(x,y)\,S_{ij}(\hat{x},\hat{x})\right]\boldsymbol{\tau}_i\cdot\boldsymbol{\tau}_j, \tag{2.33}$$

with

$$F_{\sigma\tau}(x,y) = \frac{2}{\pi}\int q^2 dq\ \mathcal{Y}_\pi(q)\ j_0(qx)\ e^{-(\sqrt{m^2+q^2/4}-m)\,y}, \tag{2.34}$$

$$F_{t\tau}(x,y) = \frac{2}{\pi}\int q^2 dq\ \mathcal{T}_\pi(q)\ j_2(qx)\ e^{-(\sqrt{m^2+q^2/4}-m)\,y}, \tag{2.35}$$

$$f(y) = \frac{m^2}{4\pi}\frac{e^{-my}}{y}, \tag{2.36}$$

$$S_{ij}(\hat{x},\hat{x}) = 3\,\boldsymbol{\sigma}_i\cdot\hat{\mathbf{x}}\,\boldsymbol{\sigma}_j\cdot\hat{\mathbf{x}} - \boldsymbol{\sigma}_i\cdot\boldsymbol{\sigma}_j. \tag{2.37}$$

In the limit $m\to\infty$, $f(y)$ becomes $\delta^3(\mathbf{y})$, $F_{\sigma\tau}(x,y)\to Y_\pi(x)$ and $F_{t\tau}(x,y)\to T_\pi(x)$. When $\mathbf{y}\to 0$, we have $\mathbf{r}'=\mathbf{r}$, $\mathbf{x}=\mathbf{r}$ and Eq. (2.33) becomes $\tilde{v}_{\pi,NR}$. Figure 6 shows $F_{\sigma\tau}(x,y)$ and $F_{t\tau}(x,y)$ as a function of x for various values of y. Note that the solid lines for $y=0$ correspond to the nonrelativistic $Y_\pi(x)$ and $T_\pi(x)$. The volume integral of $F_{\sigma\tau}(x,y)$ is independent of y, whereas that of $F_{t\tau}(x,y)$ decreases with y. Therefore relativistic effects mostly come from the tensor part of OPEP.

III. VARIATIONAL MONTE CARLO CALCULATIONS AND RESULTS

A. VMC techniques

With the relativistic Hamiltonian discussed in the previous section, we can proceed to evaluate the energy expectation value

$$\langle H_R\rangle = \langle T\rangle + \langle\tilde{v}_{ij}\rangle + \langle\delta v_{ij}\rangle + \langle\tilde{V}_{ijk}\rangle \tag{3.1}$$

for $A\geq 3$ nuclei using the Monte Carlo technique.

The Monte Carlo method [23] offers a useful way to handle the multidimensional integrals which would otherwise be impractical by the usual numerical methods. The basis of this method is that instead of integrating over a regular array of points, we sum over a set of configurations $\{\mathbf{R}_i\}$ distributed with probability $w(\mathbf{R})$. Here $\mathbf{R}=(\mathbf{r}_1,\mathbf{r}_2,\cdots,\mathbf{r}_A)$ denotes the configuration of all the nucleons in the nucleus. There are various techniques for sampling $w(\mathbf{R})$ [23], and in this work Metropolis sampling method [24] is used to treat the complicated distributions.

Variational Monte Carlo (VMC) technique is based on variational principle that the minimum expectation value of the Hamiltonian is closest to the ground state energy of the system. Starting from a variational wave function, which depends upon several variational parameters $(\alpha_1,\alpha_2,\cdots,\alpha_n)$, we evaluate the expectation value of the Hamiltonian using the Monte Carlo configuration samples $\mathbf{R}_i$:

$$\begin{aligned}\langle\hat{H}\rangle &= \frac{\int d\mathbf{R}\Psi_v^\dagger(\mathbf{R})\hat{H}\Psi_v(\mathbf{R})}{\int d\mathbf{R}\Psi_v^\dagger(\mathbf{R})\Psi_v(\mathbf{R})}\\ &= \frac{\frac{1}{N_c}\sum_{i=1}^{N_c}\left(\Psi_v^\dagger(\mathbf{R}_i)\hat{H}\Psi_v(\mathbf{R}_i)\right)/w(\mathbf{R}_i)}{\frac{1}{N_c}\sum_{i=1}^{N_c}\left(\Psi_v^\dagger(\mathbf{R}_i)\Psi_v(\mathbf{R}_i)\right)/w(\mathbf{R}_i)}\pm\delta,\end{aligned} \tag{3.2}$$

where δ is the standard deviation. Typically block averaging scheme is used to obtain a normal distribution and the error can be conveniently evaluated from it. We divide N_c configurations into N_b blocks each containing $N_0=N_c/N_b$ configurations. The average

$$\tilde{H}_b = \frac{\frac{1}{N_0}\sum_{i=1}^{N_0}\left(\Psi_v^\dagger(\mathbf{R}_i)\hat{H}\Psi_v(\mathbf{R}_i)\right)/w(\mathbf{R}_i)}{\frac{1}{N_0}\sum_{i=1}^{N_0}\left(\Psi_v^\dagger(\mathbf{R}_i)\Psi_v(\mathbf{R}_i)\right)/w(\mathbf{R}_i)} \tag{3.3}$$

is evaluated for each block. The expectation value of H is given by

$$\langle H\rangle = \frac{1}{N_b}\sum_{i=1}^{N_b}\tilde{H}_b \tag{3.4}$$

with the standard deviation

$$\delta = \frac{1}{N_b}\sqrt{\sum_{i=1}^{N_b}\left(\tilde{H}_b-\langle H\rangle\right)^2}. \tag{3.5}$$

The Monte Carlo result is exact when the number of configurations $N_c\to\infty$, although in practice N_c=50000 seems to be enough to obtain results with sufficiently small statistical errors. The weight function is usually chosen to be

$$w(\mathbf{R}_i) = \Psi_v^\dagger(\mathbf{R}_i)\Psi_v(\mathbf{R}_i) \tag{3.6}$$

to maintain small Monte Carlo error. Note that when Ψ_v is the eigenstate of H, the Monte Carlo sampling error becomes zero. Finally, the parameters $(\alpha_1,\alpha_2,\cdots,\alpha_n)$ are varied to minimize the energy.

Some of the terms in $\langle H_R \rangle$ (Eq. 3.1) can be calculated straightforwardly and have been discussed in Refs. [25] and [12]. The terms that require special techniques are the relativistic kinetic energy $\langle \sqrt{m^2 - \nabla^2} \rangle$ and $\tilde{v}_{\pi,Rel}$ in the two-body potential. The kinetic energy term has been calculated previously in Ref. [11], and the calculation of $\langle \tilde{v}_{\pi,Rel} \rangle$ is discussed in Sec. IIIC.

B. Relativistic wave functions

In the nonrelativistic case, variational wave functions of the form

$$|\Psi_v\rangle = \left(1 + \sum_{i<j<k} F_{ijk}\right) \left(\mathcal{S} \prod_{i<j} F_{ij}\right) |\Phi\rangle, \tag{3.7}$$

having symmetrized product of pair correlation operators F_{ij} and a sum of triplet correlations F_{ijk} operating on an antisymmetric, uncorrelated wave function $|\Phi\rangle$, have been commonly used. The F_{ij} and F_{ijk} correlation operators reflect the effects of two-, three-body interactions on the wave function. The uncorrelated wave function has no spatial dependence for $A \leq 4$ nuclei. A good representation of such a wave function is given in Ref. [25].

The pair correlation operator F_{ij} is constructed from correlation functions which satisfy Schrödinger-like 2-body equations, with appropriate boundary conditions. Their solutions are like deuteron wave functions Ψ_{NR} and Ψ_R displayed in Fig. 3. In the case of A=2 deuteron, both nonrelativistic and relativistic correlation functions can be easily solved in momentum space; they are not very different from each other as can be seen in Fig. 3. In $A > 2$ nuclei, the nonrelativistic pair correlation equations can be easily solved in configurations space, however, the relativistic equations are more difficult to solve. Therefore we seek good approximations for the relativistic pair correlation functions.

Our method can be easily illustrated using the example of deuteron. Its variational wave function is expressed as:

$$\Psi = \Psi_{NR} + \lambda(\Psi_R - \Psi_{NR}), \tag{3.8}$$

$\langle \Psi | H_R | \Psi \rangle$ is calculated using VMC, and λ is varied to minimize it. The results are shown in Fig. 7. The error bars shown in Fig. 7 originate from the statistical sampling and are <1% of the binding energy. The same configurations are used to calculate the energies for all λ, hence the errors are correlated. The minimum value of $\langle H_R \rangle$ does occur at $\lambda = 1$ where $\Psi = \Psi_R$ as expected. The difference in $\langle H_R \rangle$ between $\lambda = 0$ (using a nonrelativistic wave function) and $\lambda = 1$ (using a relativistic one) is ~0.04 MeV. This means that if we were to use the nonrelativistic wave function to calculate the expectation value of H_R, the result will be off by only 2% for the deuteron.

In heavier nuclei we also expect the optimum nonrelativistic wave function to provide a good approximation for relativistic wave function. The difference between the two is presumably largest in ${}^3S_1 - {}^3D_1$ and ${}^1S_0$ correlation functions at small r. We therefore define:

$$f^c_{0,1} = f^c_{0,1,NR}\ (1 + \lambda\, \xi_{{}^1S_0}), \tag{3.9}$$

$$f^c_{1,0} = f^c_{1,0,NR}\ (1 + \lambda\, \xi_{{}^3S_1}), \tag{3.10}$$

$$f^t_{1,0} = f^t_{1,0,NR}\ (1 + \lambda\, \xi_{{}^3D_1}), \tag{3.11}$$

where ξ_c for the channel c is defined as:

$$\xi_c(r) = \frac{\phi_{c,R}(r) - \phi_{c,NR}(r)}{\phi_{c,NR}(r)}. \tag{3.12}$$

At small r, the central $f^c_{1,0}$ and tensor $f^t_{1,0}$ correlation functions in spin-isospin $S, T = 1, 0$ states are proportional to the S and D radial wave functions of the deuteron, respectively. Therefore the $\xi_{{}^3S_1}$ and $\xi_{{}^3D_1}$ can be calculated exactly in momentum space using the relativistic and nonrelativistic deuteron wave functions for the $\phi_{c,R}$ and $\phi_{c,NR}$. These ξ's are rather short-ranged (Fig. 8), and we do not expect them to vary significantly in larger nuclei. Wiringa [4] has shown that the nonrelativistic correlation functions for ^{2}H, ^{3}H and ^{4}He are almost the same at small r.

A similar calculation of $\xi_{{}^1S_0}$ is not possible because of the absence of a bound state in that channel. However, we can obtain an artificial ${}^1S_0$ bound state by slightly increasing

the strength of intermediate range attraction in $v(^1S_0)$. The binding energy and the wave function at large r are very sensitive to small changes in $v(^1S_0)$, however, $\xi_{^1S_0}$ is relatively insensitive. As an example, the $\xi_{^1S_0}$ obtained from artificial $^1S_0$ bound states with energies of -1 and -10 MeV, shown in Fig. 8, are very similar.

The VMC energy of ^{3}H with the relativistic Hamiltonian is shown as a function of λ in Fig. 9. The minimum occurs at λ=0.5 instead of 1 (the expected value), however, the difference in $\langle H_R \rangle$ between λ=0.5 and 1 is rather small and of the order of the Monte Carlo sampling error. The minimum energy for ^{4}He occurs at the expected λ=1.0.

C. Expectation value of the nonlocal potential

Consider an A-nucleon system whose wave function is denoted as $\Psi(\mathbf{r}_1, \mathbf{r}_2, \cdots, \mathbf{r}_A)$. We define:

$$\mathbf{x}_i = \frac{1}{2}(\mathbf{r}_i + \mathbf{r}'_i), \qquad \mathbf{x}_j = \frac{1}{2}(\mathbf{r}_j + \mathbf{r}'_j), \tag{3.13}$$

so that

$$\mathbf{x} = \mathbf{x}_i - \mathbf{x}_j, \qquad \frac{\mathbf{y}}{2} = \mathbf{r}_i - \mathbf{r}'_i = \mathbf{r}'_j - \mathbf{r}_j, \tag{3.14}$$

as illustrated in Fig. 10. The expectation value of relativistic OPEP is then given by

$$\begin{aligned}\langle \tilde{v}_{\pi,Rel} \rangle = \sum_{i<j} \int \prod_{k\neq i,j} \mathrm{d}^3 r_k \mathrm{d}^3 x_i \mathrm{d}^3 x_j \mathrm{d}^3 y \;\; \Psi^\dagger \left(\mathbf{r}_1, \cdots, \mathbf{x}_i - \frac{\mathbf{y}}{4}, \cdots, \mathbf{x}_j + \frac{\mathbf{y}}{4}, \cdots, \mathbf{r}_A\right) \\ \tilde{v}_{\pi,Rel}\left(|\mathbf{x}_i - \mathbf{x}_j|, y\right) \;\; \Psi \left(\mathbf{r}_1, \cdots, \mathbf{x}_i + \frac{\mathbf{y}}{4}, \cdots, \mathbf{x}_j - \frac{\mathbf{y}}{4}, \cdots, \mathbf{r}_A\right),\end{aligned} \tag{3.15}$$

where $\tilde{v}_{\pi,Rel}\left(|\mathbf{x}_i - \mathbf{x}_j|, y\right)$ is previously calculated in Eq. (2.33). The integration over the $\mathbf{r}_k$'s, $\mathbf{x}_i$, $\mathbf{x}_j$ and the solid angle of $\mathbf{y}$ is carried out by the Monte Carlo method, while that over the magnitude of y is carried out with Gauss-Laguerre integral.

D. VMC results

The VMC results for ^{3}H and ^{4}He are listed in Table IV. Note that in principle we should use GFMC to calculate the exact binding energies, but the relativistic effects resulting from

the difference between $\langle H_R \rangle$ and $\langle H_{NR} \rangle$ are small and presumably not too different from those estimated using VMC.

The total relativistic effect on the binding energy is ~0.3 MeV for ^{3}H and ~1.8 MeV for ^{4}He. Most of the effect comes from the boost correction which is 0.42 MeV for ^{3}H and 1.94 MeV for ^{4}He. The net effect of relativistic corrections to the kinetic energy and the two-body potential, on the binding energy is rather small: $\sim -0.12 \pm 0.06$ MeV in (^{3}H) and $\sim -0.17 \pm 0.10$ MeV in (^{4}He). Since both H_{NR} and H_R are constrained to give the same deuteron binding energy, the changes in $\langle T \rangle$ and $\langle \tilde{v}_{ij} \rangle$ cancel exactly in ^{2}H. In ^{3}H and ^{4}He they appear to largely cancel and give a rather small net effect.

In view of the slow convergence of the $\langle |\tilde{v}_{\pi,Rel} - \tilde{v}_{\pi,NR}| \rangle$, when expanded in powers of p^2/m^2, one may question the validity of calculating the boost interaction δv only up to first order in $P^2/4m^2$. The average kinetic energies of nucleons in nuclei are rather small giving average $p_i^2/m^2 < 0.1$. The expansion has good convergence for such values. However, two nucleons can occasionally have large relative momenta when they come close together as illustrated in Fig. 11. In that configuration $\mathbf{p}_i \sim \mathbf{p}$ and $\mathbf{p}_j \sim -\mathbf{p}$ are both large due to strong short-range interaction between nucleons i and j. Such configurations are responsible for the slow convergence of the expansion of $\langle |\tilde{v}_{\pi,Rel} - \tilde{v}_{\pi,NR}| \rangle$. In these configurations the squares of the total pair momenta are of order $P_{ik}^2 \sim P_{jk}^2 \sim p^2$, while P_{ij}^2 has small, near average value. Thus the expansion parameter $P^2/4m^2$ for the boost interaction is effectively four times smaller than that of $(\tilde{v}_{\pi,Rel} - \tilde{v}_{\pi,NR})$ when the momenta are generated by pair correlations, therefore we expect the boost expansion to converge more rapidly. Moreover, $\langle |\tilde{v}_{\pi,Rel} - \tilde{v}_{\pi,NR}| \rangle$ is much larger ($\sim$ 6 and 13 MeV in ^{3}H and ^{4}He respectively) than $\langle |\delta v| \rangle$ and has to be calculated with higher relative accuracy to obtain a final total energy with error $\sim$ 1 %.

IV. CONCLUSIONS AND OUTLOOK

We find that the relativistic effects in on-shell OPEP are quite substantial. The expectation values of $\tilde{v}_{\pi,Rel}$ are smaller than those of $\tilde{v}_{\pi,NR}$ by $\sim$ 15 %. Since the expectation values of OPEP are much larger than nuclear binding energies, the differences in the OPEP expectation values are comparable to the total nuclear energy. However, nuclear Hamiltonians are not derived from first principles, they are obtained by fitting data. The substantial difference between $\tilde{v}_{\pi,Rel}$ and $\tilde{v}_{\pi,NR}$ is compensated in the H_{NR} by that in the kinetic energy T and $\tilde{v}_R$ so that it gives the same scattering cross sections and deuteron energy as the H_R. We find that this compensation works rather well for three- and four-body nuclei. In absence of the boost interaction our nonrelativistic and relativistic Hamiltonians seem to give very similar results for the binding energies and wave functions of light nuclei. It is probably necessary to examine one-pion exchange current contributions to elastic scattering form factors and radiative capture reactions to see the effect of the m/E factors in the OPEP.

The modern two-nucleon potential models, which include the Nijmegen models I, II and Reid-93 [26], Argonne v_{18} [6] and CD-Bonn [27], accurately reproduce the NN-scattering data in the Nijmegen data base. Friar *et al.* [28] have studied the triton energy with the Nijmegen and Argonne models, without boost or three-nucleon interactions, using accurate Faddeev calculations. The energies obtained with the three local potential models, Reid-93, Nijmegen-II and Argonne v_{18} are respectively -7.63, -7.62 and -7.61 MeV. These energies are very close, and these models also give very similar values (5.70, 5.64 and 5.76 %) for P_D, the fraction of D-state in the deuteron. The boson exchange Nijmegen-I model contains nonlocal terms and gives -7.72 MeV for triton energy and 5.66% for P_D. Comparison of the results of Nijmegen I and II models indicates that the total effect of the nonlocalities on energies and the wave functions could be small. The present results support this conclusion; inclusion of relativistic nonlocalities in on-shell OPEP and kinetic energy lowers the triton energy by $\sim$ 0.1 MeV and P_D by 0.04%.

In contrast the CD-Bonn potential gives rather different results from the Nijmegen and

Argonne models. It gives a triton energy of -8.00 MeV and P_D = 4.83%. The OPEP in the CD-Bonn model has additional off-shell nonlocalities which disappear in the on-shell relativistic OPEP. It is defined as [29]:

$$\tilde{v}_{\pi,CDB}(\mathbf{p}',\mathbf{p}) = -\frac{f_{\pi NN}^2}{\mu^2}\,\frac{\boldsymbol{\tau}_i\cdot\boldsymbol{\tau}_j}{\mu^2+q^2}\,\frac{m}{E}\,\frac{m}{E'}\,\Big[\boldsymbol{\sigma}_i\cdot\mathbf{q}\;\boldsymbol{\sigma}_j\cdot\mathbf{q} + (E'-E)\left(\frac{\boldsymbol{\sigma}_i\cdot\mathbf{p}\;\boldsymbol{\sigma}_j\cdot\mathbf{p}}{E+m} - \frac{\boldsymbol{\sigma}_i\cdot\mathbf{p}'\;\boldsymbol{\sigma}_j\cdot\mathbf{p}'}{E'+m}\right)\Big], \tag{4.1}$$

where $E = \sqrt{m^2+p^2}$, $E' = \sqrt{m^2+p'^2}$. The term proportional to $(E'-E)$ does not contribute to the on-shell OPEP, and is absent from our $\tilde{v}_{\pi,Rel}$ given by Eq. (2.5). The OPEP gives large contributions by coupling states with small p to large p'. Therefore we consider the case $p=0$ for which $\mathbf{p}' = -\mathbf{q}$, and expand in powers of q^2/m^2. This gives:

$$\tilde{v}_{\pi,CDB}(\mathbf{q},0) = \tilde{v}_{\pi,NR}\left(1-\frac{3q^2}{4m^2}+\cdots\right), \tag{4.2}$$

$$\tilde{v}_{\pi,Rel}(\mathbf{q},0) = \tilde{v}_{\pi,NR}\left(1-\frac{q^2}{2m^2}+\cdots\right), \tag{4.3}$$

indicating presence of larger relativistic corrections in the $\tilde{v}_{\pi,CDB}$.

The second order contributions of the $\tilde{v}_{\pi,CDB}$ provide a sightly better approximation to the sum of the twelve time-ordered two-pion exchange diagrams [22] with only positive energy nucleons in the intermediate states, in relativistic field theories with pseudoscalar coupling. The two-pion exchange diagrams with antinucleons are discarded on arguments based on chiral symmetry. It is not obvious that this off-shell term must be retained, and not discarded. It is necessary to find experimental tests for its existence, as well as for the suppression of OPEP by m/E factors considered in this work.

The off-shell behavior of the OPEP can also be changed by using combinations of pseudoscalar and pseudovector couplings. In Friar's notation [30] the possible off-shell behaviors are characterized with parameters $\tilde{\mu}$ and ν, and up to order p^2/m^2 they are related by unitary transformations. Up to this order our $\tilde{v}_{\pi,Rel}$ has an off-shell behavior with $\nu = 1/2$ and $\tilde{\mu} = 0$, while that of $\tilde{v}_{\pi,CDB}$ has $\nu = 1/2$ and $\tilde{\mu} = -1$. The P_D has smaller values for $\tilde{\mu} = -1$ [31] used in the CD-Bonn potential.

The boost interaction δv gives the dominant relativistic correction to the binding energies of light nuclei in the present formalism. Contributions of δv are very small, only ~ 1 % of that of $\tilde{v}$ in ^{3}H and ^{4}He. However they are not canceled by relativistic effects in either T or $\tilde{v}$, and therefore dominate the net effect. Like the two-nucleon, the three-nucleon interaction is also not derived from first principles. Urbana models of V_{ijk} contain two terms: the attractive two-pion exchange term $V_{ijk}^{2\pi}$ and a repulsive phenomenological term V_{ijk}^{R}. Their strengths are chosen to reproduce the triton energy and the density of nuclear matter without considering any relativistic effects. In light nuclei the repulsive $\delta\tilde{v}$ contribution is about 37 % of that of V_{ijk}^{R}. Thus the strength of V_{ijk}^{R} in H_R has to be reduced by 37 % to obtain the experimental energies of light nuclei. One could also choose to increase the strength of $V_{ijk}^{2\pi}$ or some combination of increasing $V_{ijk}^{2\pi}$ and decreasing V_{ijk}^{R}, but in this work we keep $V_{ijk}^{2\pi}$ unchanged. The difference in the three nucleon interaction then compensates for the omission of δv in conventional nonrelativistic nuclear Hamiltonians. It appears that this compensation works rather well in light nuclei having up to eight nucleons [32], as well as in nuclear and neutron matter up to normal densities [33]. It presumably works also in heavier nuclei where it is not tested. However, at several times nuclear matter densities, encountered in neutron stars, the effective three-nucleon interaction overestimates the δv contribution significantly [33].

ACKNOWLEDGMENTS

The authors would like to thank J. Carlson, R. Schiavilla for many interesting discussions, R. B. Wiringa for his help on the nonrelativistic variational wave function. A.A. acknowledges the kind hospitality of the Physics Department of the University of Illinois at Urbana-Champaign, where large part of this work has been performed. The calculations were performed on IBM SP machines at Cornell Theory Center, and on Cray supercomputers at Pittsburgh Supercomputing Center. This work was supported by the U.S. National Science Foundation under Grant PHY94-21309, and the work of A.A. by Universidade de Lisboa, Junta de Investigação Científica e Tecnológica under contract No. PBIC/C/CEN/1108/92.

APPENDIX A: RELATIVISTIC OPEP IN CONFIGURATION SPACE

The third term in Eq. (2.27) gives the second-order relativistic correction to OPEP and is denoted as $v^{(2)}$:

$$v^{(2)}(\mathbf{x},\mathbf{y}) = \int \frac{\mathrm{d}^3Q}{(2\pi)^3}\frac{\mathrm{d}^3q}{(2\pi)^3} g(q,Q)\cos^2\theta_{qQ}\tilde{v}_{\pi,NR}(\mathbf{q})\mathrm{e}^{i(\mathbf{Q}\cdot\mathbf{y}+\mathbf{q}\cdot\mathbf{x})} \tag{A1}$$

where θ_{qQ} is the angle between $\mathbf{q}$ and $\mathbf{Q}$, and

$$g(q,Q) = \frac{1}{2}\frac{m^2Q^2q^2}{(m^2+Q^2+\frac{q^2}{4})^3} \tag{A2}$$

Expressing $\cos^2\theta_{qQ}$ as

$$\cos^2\theta_{qQ} = \frac{2}{3}\mathrm{P}_2(\cos\theta_{qQ}) + \frac{1}{3}, \tag{A3}$$

we get

$$\begin{aligned} v^{(2)}(\mathbf{x},\mathbf{y}) = {} & \frac{1}{3}\int \frac{\mathrm{d}^3Q}{(2\pi)^3}\frac{\mathrm{d}^3q}{(2\pi)^3} g(q,Q)\,\tilde{v}_{\pi,NR}(\mathbf{q})\,\mathrm{e}^{i(\mathbf{Q}\cdot\mathbf{y}+\mathbf{q}\cdot\mathbf{x})} \\ & + \frac{2}{3}\int \frac{\mathrm{d}^3Q}{(2\pi)^3}\frac{\mathrm{d}^3q}{(2\pi)^3} g(q,Q)\,\mathrm{P}_2(\cos\theta_{qQ})\,\tilde{v}_{\pi,NR}(\mathbf{q})\,\mathrm{e}^{i(\mathbf{Q}\cdot\mathbf{y}+\mathbf{q}\cdot\mathbf{x})}. \end{aligned} \tag{A4}$$

The first integral denoted by $v_1^{(2)}(\mathbf{x},\mathbf{y})$ is independent of θ_{qQ} and can be easily evaluated by using Eq. (2.30) and the following identities:

$$e^{i\mathbf{q}\cdot\mathbf{r}} = 4\pi\sum_{lm} i^l Y^*_{lm}(\hat{q})Y_{lm}(\hat{r})j_l(qr), \tag{A5}$$

$$\int Y^*_{lm}(\hat{q})Y_{l'm'}(\hat{q})\mathrm{d}\Omega_q = \delta_{ll'}\delta_{mm'}, \tag{A6}$$

$$\int v(r)\boldsymbol{\sigma}_i\cdot\hat{r}\boldsymbol{\sigma}_j\cdot\hat{r}\; e^{i\mathbf{q}\cdot\mathbf{r}}\mathrm{d}^3r = -\boldsymbol{\sigma}_i\cdot\boldsymbol{\nabla}_q\boldsymbol{\sigma}_j\cdot\boldsymbol{\nabla}_q\int v(r)e^{i\mathbf{q}\cdot\mathbf{r}}\frac{1}{r^2}\mathrm{d}^3r. \tag{A7}$$

We obtain:

$$\begin{aligned} v_1^{(2)}(\mathbf{x},\mathbf{y}) = \frac{\mu}{9\pi^3}\frac{f_{\pi NN}^2}{4\pi}\Big[& \int Q^2\mathrm{d}Qq^2\mathrm{d}q\, g(q,Q)\,\mathcal{Y}_\pi(q)\,j_0(Qy)j_0(qx)\,\boldsymbol{\sigma}_i\cdot\boldsymbol{\sigma}_j \\ & + \int Q^2\mathrm{d}Qq^2\mathrm{d}q\, g(q,Q)\,\mathcal{T}_\pi(q)\,j_0(Qy)j_2(qx)\,S_{ij}(\hat{x},\hat{x})\Big]\boldsymbol{\tau}_i\cdot\boldsymbol{\tau}_j \end{aligned} \tag{A8}$$

where $\mathcal{Y}_\pi(q)$ and $\mathcal{T}_\pi(q)$ are previously given in Eqs. (2.31) and (2.32).

To calculate the second integral in Eq. (A4), we use

$$\mathrm{P}_l(\cos\theta_{qQ}) = \frac{4\pi}{2l+1}\sum_m Y^*_{lm}(\hat{Q})Y_{lm}(\hat{q}). \tag{A9}$$

The integral over the solid angles becomes:

$$\int \mathrm{d}\Omega_Q\mathrm{d}\Omega_q e^{i(\mathbf{Q}\cdot\mathbf{y}+\mathbf{q}\cdot\mathbf{x})}\mathrm{P}_2(\cos\theta_{qQ}) = (4\pi)^2\mathrm{P}_2(\cos\theta_{xy})j_2(Qy)j_2(qx), \tag{A10}$$

and the second term in Eq. (A4), denoted by $v_2^{(2)}(\mathbf{x},\mathbf{y})$ is:

$$\begin{aligned} v_2^{(2)}(\mathbf{x},\mathbf{y}) = {} & \frac{2\mu}{9\pi^3}\frac{f_{\pi NN}^2}{4\pi}\Big\{\mathrm{P}_2(\cos\theta_{xy})\int Q^2\mathrm{d}Qq^2\mathrm{d}q g(q,Q)\,[\mathcal{Y}_\pi(q)+\mathcal{T}_\pi(q)]\,j_2(Qy)j_2(qx)\boldsymbol{\sigma}_i\cdot\boldsymbol{\sigma}_j, \\ & + 3\boldsymbol{\sigma}_i\cdot\boldsymbol{\nabla}_x\boldsymbol{\sigma}_j\cdot\boldsymbol{\nabla}_x\Big[\mathrm{P}_2(\cos\theta_{xy})\int Q^2\mathrm{d}Q\mathrm{d}qg(q,Q)\mathcal{T}_\pi(q)j_2(Qy)j_2(qx)\Big]\Big\}\boldsymbol{\tau}_i\cdot\boldsymbol{\tau}_j. \end{aligned} \tag{A11}$$

Here θ_{xy} is the angle between $\mathbf{x}$ and $\mathbf{y}$. The gradient operators $\boldsymbol{\nabla}_x$ in the second term act on both $\mathrm{P}_2(\cos\theta_{xy})$ and $j_2(qx)$.

The Q-integral in Eqs. (A8) and (A11) can be performed analytically and results

$$\int Q^2\mathrm{d}Q\, g(q,Q)\, j_0(Qy) = f(y)\,[Z_2(q,y) - Z_1(q,y))], \tag{A12}$$

$$\int Q^2\mathrm{d}Q\, g(q,Q)\, j_2(Qy) = f(y)Z_1(q,y), \tag{A13}$$

where f(y) is the Yukawa function given in Eq.(2.33) and

$$Z_1(q,y) = \frac{(\pi qy)^2}{8}\,\mathrm{e}^{-(\sqrt{m^2+\frac{q^2}{4}}-m)y}, \tag{A14}$$

$$Z_2(q,y) = \frac{3}{\sqrt{m^2+\frac{q^2}{4}}\,y}\,Z_1(q,y). \tag{A15}$$

$v^{(2)}$ is finally obtained as:

$$\begin{aligned} v^{(2)}(\mathbf{x},\mathbf{y}) = \frac{\mu}{3}\frac{f_{\pi NN}^2}{4\pi}f(y)[& I_1(x,y,\theta_{xy})\,\boldsymbol{\sigma}_i\cdot\boldsymbol{\sigma}_j + I_2(x,y,\theta_{xy})\,S_{ij}(\hat{x},\hat{x}) + \\ & I_3(x,y,\theta_{xy})\,S_{ij}(\hat{y},\hat{y}) + I_4(x,y,\theta_{xy})\,S_{ij}(\hat{x},\hat{y})]\boldsymbol{\tau}_i\cdot\boldsymbol{\tau}_j, \end{aligned} \tag{A16}$$

where the tensor operator $S_{ij}(\hat{x},\hat{y})$ is defined as:

$$S_{ij}(\hat{x},\hat{y}) = \frac{3}{2}\,(\boldsymbol{\sigma}_i\cdot\hat{x}\boldsymbol{\sigma}_j\cdot\hat{y} + \boldsymbol{\sigma}_i\cdot\hat{y}\boldsymbol{\sigma}_j\cdot\hat{x}) - \hat{x}\cdot\hat{y}\,\boldsymbol{\sigma}_i\cdot\boldsymbol{\sigma}_j, \tag{A17}$$

and I_1, I_2, I_3 and I_4 are given by:

$$I_1(x,y,\theta_{xy}) = \mathcal{F}^{\mathcal{Y}}_{20}(x,y) - \mathcal{F}^{\mathcal{Y}}_{10}(x,y) + 2\,\mathcal{F}^{\mathcal{Y}}_{12}(x,y)\,\mathrm{P}_2(\cos\theta_{xy}) \tag{A18}$$

$$I_2(x,y,\theta_{xy}) = \mathcal{F}^{\mathcal{T}}_{22}(x,y) - 3\,\mathcal{H}^{\mathcal{T}}_{13}(x,y) + 3\,\mathcal{F}^{\mathcal{T}}_{14}(x,y)\,\cos^2\theta_{xy} \tag{A19}$$

$$I_3(x,y,\theta_{xy}) = 6\,\mathcal{H}^{\mathcal{T}}_{12}(x,y) \tag{A20}$$

$$I_4(x,y,\theta_{xy}) = -12\,\mathcal{H}^{\mathcal{T}}_{13}(x,y)\cos\theta_{xy} \tag{A21}$$

where

$$\mathcal{F}^{\mathcal{Y}}_{\alpha l}(x,y) = \frac{1}{3\pi^3}\int q^2 \mathrm{d}q Z_\alpha(q,y)\,\mathcal{Y}_\pi(q)\,j_l(qx) \tag{A22}$$

$$\mathcal{F}^{\mathcal{T}}_{\alpha l}(x,y) = \frac{1}{3\pi^3}\int q^2 \mathrm{d}q Z_\alpha(q,y)\,\mathcal{T}_\pi(q)\,j_l(qx) \tag{A23}$$

$$\mathcal{H}^{\mathcal{T}}_{\alpha l}(x,y) = \frac{1}{3\pi^3}\int q^2 \mathrm{d}q Z_\alpha(q,y)\,\mathcal{T}_\pi(q)\,\frac{j_l(qx)}{(qx)^{4-l}} \tag{A24}$$

REFERENCES

* Current address: Jefferson Lab Theory Group, 12000 Jefferson Ave, Newport News, VA 23606. Electronic address: jforest@jlab.org.

† Electronic address: vijay@rsm1.physics.uiuc.edu

‡ Electronic address: arriaga@alf1.cii.fc.ul.pt

[1] W. Glöckle and H. Kamada, Phys. Rev. Lett. **71**, 971 (1993).

[2] A. Kievsky, M. Viviani, and S. Rosati, Nucl. Phys. **A551**, 241 (1993); **A577**, 511 (1994).

[3] J. Carlson, in *Structure of Hadrons and Hadronic matter*, ed. O. Scholten and J. H. Koch, World Scientific, 1991, p.43.

[4] R. B. Wiringa, Phys. Rev. C **43**, 1585 (1991).

[5] B. S. Pudliner, V. R. Pandharipande, J. Carlson and R. B. Wiringa, Phys. Rev. Lett. **74**, 4396 (1995); B. S. Pudliner, V. R. Pandharipande, J. Carlson, Steven C. Pieper and R. B. Wiringa, Phys. Rev. C **56**, 1720 (1997).

[6] R. B. Wiringa, V. G. J. Stoks, R. Schiavilla, Phys. Rev. C **51**, 38 (1995). Phys. Rev. C **54**, 646 (1996).

[7] G. Rupp and J. A. Tjon, Phys. Rev. C **45**, 2133 (1992).

[8] F. Sammarruca and R. Machleidt, Preprint nucl-th/9606047, in press in *Few-Body Systems.*

[9] Alfred Stadler and Franz Gross, Phys. Rev. Lett. **78**, 26 (1997).

[10] B. D. Keister and W. N. Polyzou, *Adv. Nucl. Phys.* **20**, 225 (1991).

[11] J. Carlson, V. R. Pandharipande and R. Schiavilla, Phys. Rev. C **47**, 484 (1993).

[12] J. L. Forest, V. R. Pandharipande, J. Carlson and R. Schiavilla, Phys. Rev. C **52**, 576 (1995).

[13] B. Bakamjian and L. H. Thomas, Phys. Rev. **92**, 1300 (1952).

[14] L. L. Foldy, Phys. Rev. **122**, 275 (1961).

[15] R. A. Krajcik and L. L. Foldy, Phys. Rev. D **10**, 1777 (1974).

[16] J. L. Friar, Phys. Rev. C **12**, 695 (1975).

[17] J. L. Forest, V. R. Pandharipande and J. L. Friar, Phys. Rev. C **52**, 568 (1995).

[18] H. Kamada and W. Glöckle, Phys. Rev. Lett. **80**, 2547 (1998).

[19] V. G. J. Stoks, R. A. M. Klomp, M. C. M. Rentmeester and J. J. de Swart, Phys. Rev. C **48**, 792 (1993).

[20] W. Glöckle, T.-S.H. Lee and F. Coester, Phys. Rev. C **33**, 709 (1986).

[21] R. Machleidt, K. Holinde and Ch. Elster, Phys. Rep. 149, 1 (1987).

[22] R. A. Smith and V. R. Pandharipande, Nucl. Phys. **A256**, 327 (1976).

[23] M. H. Kalos and P. A. Whitlock, *Monte Carlo Methods*, Wiley (1986).

[24] N. Metropolis *et al.*, J. Chem. Phys. **21**, 1087 (1953).

[25] A. Arriaga, V.. R. Pandharipande, and R. B. Wiringa, Phys. Rev. C **52**, 2362 (1995).

[26] V. G. J. Stoks, R. A. M. Klomp, C. P. F. Terheggen and J. J. de Swart, Phys. Rev. C **49**, 2950 (1994).

[27] R. Machleidt, F. Sammarruca and Y. Song, Phys. Rev. C **53**, R1483-R1487 (1996).

[28] J. L. Friar, G. L. Payne, V.G.J. Stoks and J.J. de Swart, Phys. Lett. **B331**, 4 (1993).

[29] R. Machleidt, private communication (1997).

[30] J. L. Friar, Phys. Rev. C **22**, 796 (1980).

[31] J. Adam, Jr., H. Goller and H. Arenhovel, Phys. Rev. C **48**, 370 (1993).

[32] S. C. Pieper, private communication (1998).

[33] A. Akmal, V. R. Pandharipande and D. G. Ravenhall, preprint nucl-th/9804027 (1998).

FIGURES

FIG. 1. Phase shifts as a function of lab energy. $\diamond$: the reference phase shifts obtained with H_{NR}; +: those using $\tilde{v}_R$ from H_{NR} in H_R; $\Box$: those with the new relativistic Hamiltonian H_R with re-adjusted $\tilde{v}_R$.

FIG. 2. Comparison of relativistic (solid lines) and nonrelativistic (dashed lines) potentials $v_1 - v_{14}$ of the operator format (refer to Eq. 2.12). Note that v_4 and v_6 contain contributions from both $\tilde{v}_\pi$ and $\tilde{v}_R$, and only a local nonrelativistic OPEP is used.

FIG. 3. Deuteron wave functions.

FIG. 4. Deuteron wave functions in momentum space.

FIG. 5. Ratio of deuteron relativistic to nonrelativistic D-wave function in momentum space (solid line), and the simple estimate of Eq. 2.22 (dashed line). The dotted and dot-dashed lines represent results calculated using T_{NR}, $\tilde{v}_{\pi,Rel}$ and T_{Rel}, $\tilde{v}_{\pi,NR}$ in $\phi_{D,Rel}$ in Eq. (2.22), respectively. The wiggle in the calculated ratio around 7 fm^{-1} comes from a node in the wave function.

FIG. 6. $F_{\sigma\tau}$ and $F_{t\tau}$ as a function of x for various values of y.

FIG. 7. VMC results for deuteron with 100,000 configurations.

FIG. 8. $\xi = \frac{f_R - f_{NR}}{f_{NR}}$ as a function of r.

FIG. 9. VMC results for triton with 50,000 configurations.

FIG. 10. A diagram to illustrate the calculation of nonlocal interaction contributions.

FIG. 11. A naive picture of ^{3}H to illustrate large momentum contribution from a configuration where two nucleons are close together.

TABLES

TABLE I. Nonrelativistic Green's Function Monte Carlo (GFMC) results (in MeV) for light nuclei with the Argonne v_{18} and Urbana IX potentials. The first line gives the experimental energy while the next four list the calculated total, kinetic, two- and three-body interaction energies. The last two lines give the contribution of the pion exchange parts of 2- and 3-body interactions.

	^{2}H	^{3}H	^{4}He	^{6}Li	^{7}Li	^{8}Be
E_{exp}	-2.2246	-8.48	-28.30	-31.99	-39.24	-56.50
$< E >$	-2.2248(5)	-8.47(1)	-28.30(2)	-31.25(11)	-37.44(28)	-54.66(64)
$< T >$	19.81	50.8(5)	111.9(6)	150.8(10)	186.4(28)	246.3(56)
$< v_{ij} >$	-22.04	-58.4(5)	-135.4(6)	-179.2(10)	-220.8(30)	-295.8(62)
$< V_{ijk} >$	0.0	-1.20(2)	-6.4(1)	-7.2(1)	-8.9(2)	-14.8(5)
$< v_\pi >$	-21.28	-43.8(2)	-99.4(2)	-128.9(5)	-152.5(7)	-224.1(9)
$< V^{2\pi} >$	0.0	-2.17(1)	-11.7(1)	-13.5(1)	-17.1(4)	-28.1(8)

TABLE II. Deuteron properties

	H_{NR}	H_R
binding energy (MeV)†	-2.242	-2.242
quadrupole moment (fm^2)	0.269	0.271
% of D state (P_D)	5.776	5.732

† without electromagnetic interactions

TABLE III. Results of momentum space deuteron calculations.

	$\langle\Psi_{NR}\|H_{NR}\|\Psi_{NR}\rangle$	$\langle\Psi_R\|H_R\|\Psi_R\rangle$
$\langle E\rangle$	-2.242	-2.242
$\langle T\rangle$	19.882	18.877
$\langle\tilde{v}_{ij}\rangle$	-22.125	-21.119
$\langle\tilde{v}_\pi\rangle$	-21.356	-18.797
$\langle\tilde{v}_R\rangle = \langle\tilde{v}_{ij} - \tilde{v}_\pi\rangle$	-0.769	-2.322
$\langle\tilde{v}_{\pi,Rel} - \tilde{v}_{\pi,NR}\rangle$		2.589

TABLE IV. VMC results for ^{3}H and ^{4}He, calculated with 50,000 configurations.

	^{3}H			^{4}He		
	H_{NR}	H_R	$H_R - H_{NR}$	H_{NR}	H_R	$H_R - H_{NR}$
$\langle E\rangle$†	-8.24(3)	-7.94(4)	0.30(5)	-28.09(7)	-26.32(8)	1.8(1)
$\langle T\rangle$	50.1(5)	48.6(5)	-1.5(7)	104.8(9)	98.4(8)	-6(1)
$\langle\tilde{v}_{ij}\rangle$	-57.3(5)	-56.0(5)	1.3(7)	-127.6(9)	-121.5(9)	6(1)
$\langle\tilde{V}_{ijk}\rangle$	-1.06(3)	-1.03(3)		-5.29(9)	-5.20(8)	
$\langle\delta v_{ij}\rangle$		0.42(1)			1.94(3)	
$\langle\tilde{V}^R_{ijk}\rangle$	0.98(3)	1.01(3)		5.26(7)	5.38(8)	
$\langle\tilde{v}_\pi\rangle$	-44.0(2)	-38.3(2)	5.7(4)	-97.1(5)	-83.8(4)	13.3(1)

† without electromagnetic interaction

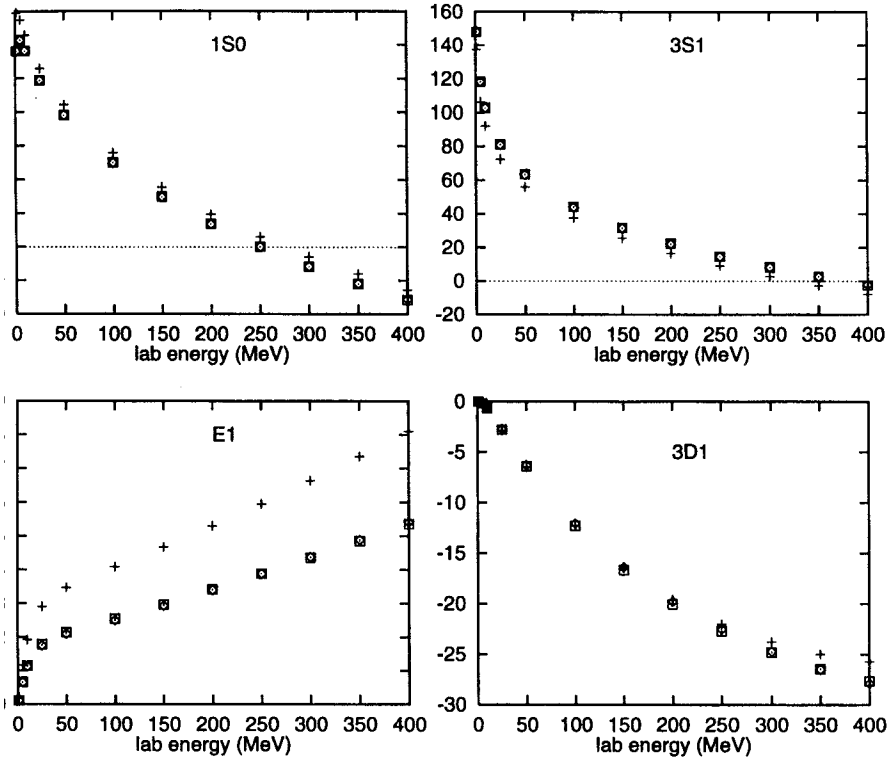
1S0
3S1
E1
3D1
lab energy (MeV)

Fig. 1

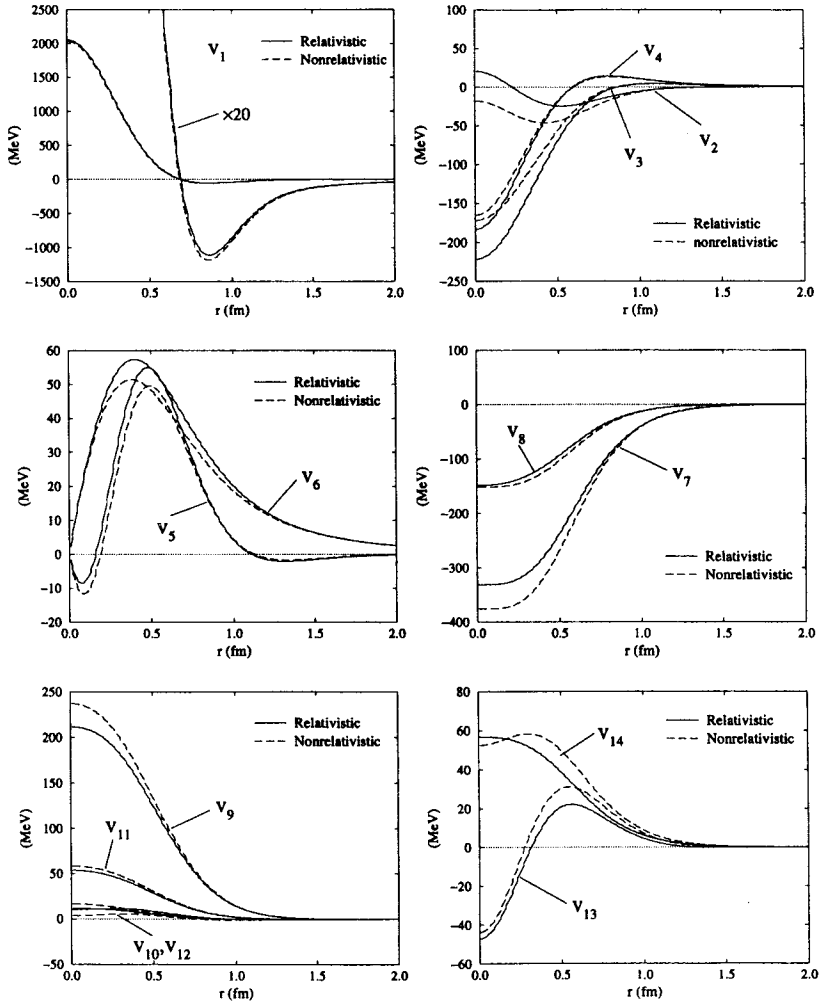
V1
×20
V4
V3
V2
V6
V5
V8
V7
V9
V11
V10,V12
V14
V13
Relativistic
Nonrelativistic
(MeV)
r (fm)

Fig. 2

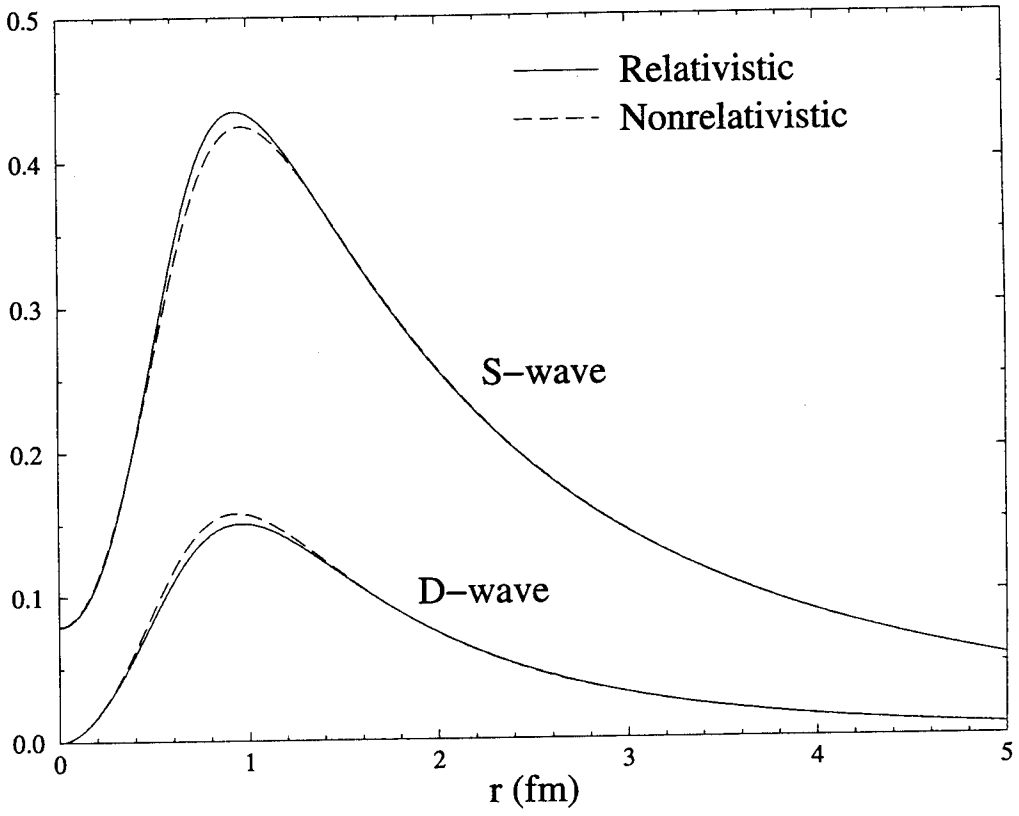
0.5
0.4
0.3
0.2
0.1
0.0
0
1
2
3
4
5
r (fm)
Relativistic
Nonrelativistic
S–wave
D–wave

Fig. 3

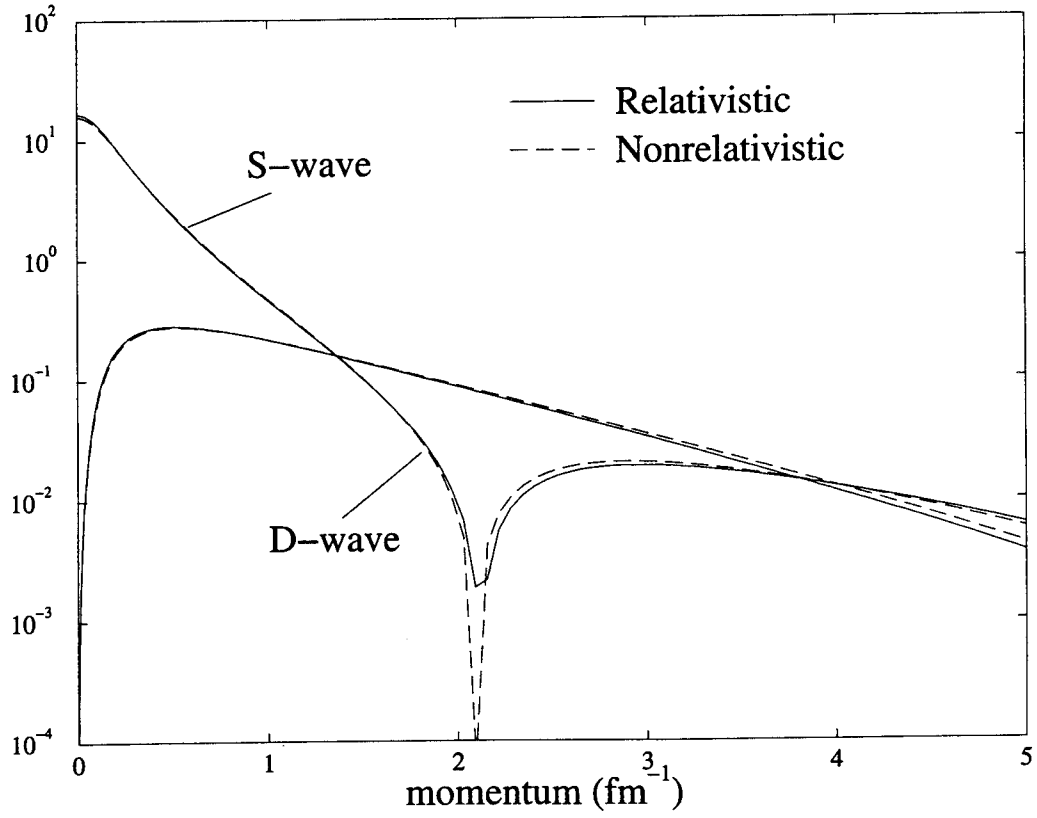
10^2
10^1
10^0
10^{-1}
10^{-2}
10^{-3}
10^{-4}
0
1
2
3
4
5
momentum (fm^{-1})
Relativistic
Nonrelativistic
S–wave
D–wave

Fig. 4

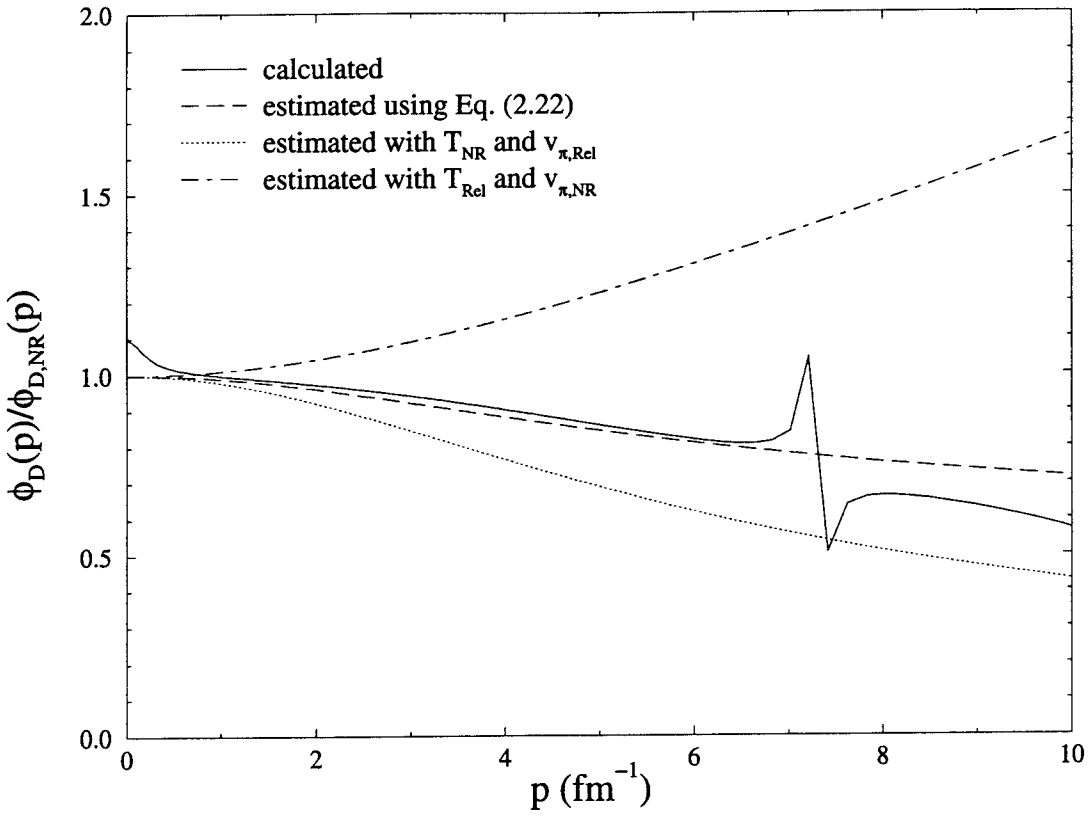
calculated
estimated using Eq. (2.22)
estimated with T_{NR} and $v_{\pi,Rel}$
estimated with T_{Rel} and $v_{\pi,NR}$
$\phi_D(p)/\phi_{D,NR}(p)$
p (fm^{-1})
0.0
0.5
1.0
1.5
2.0
0
2
4
6
8
10

Fig. 5

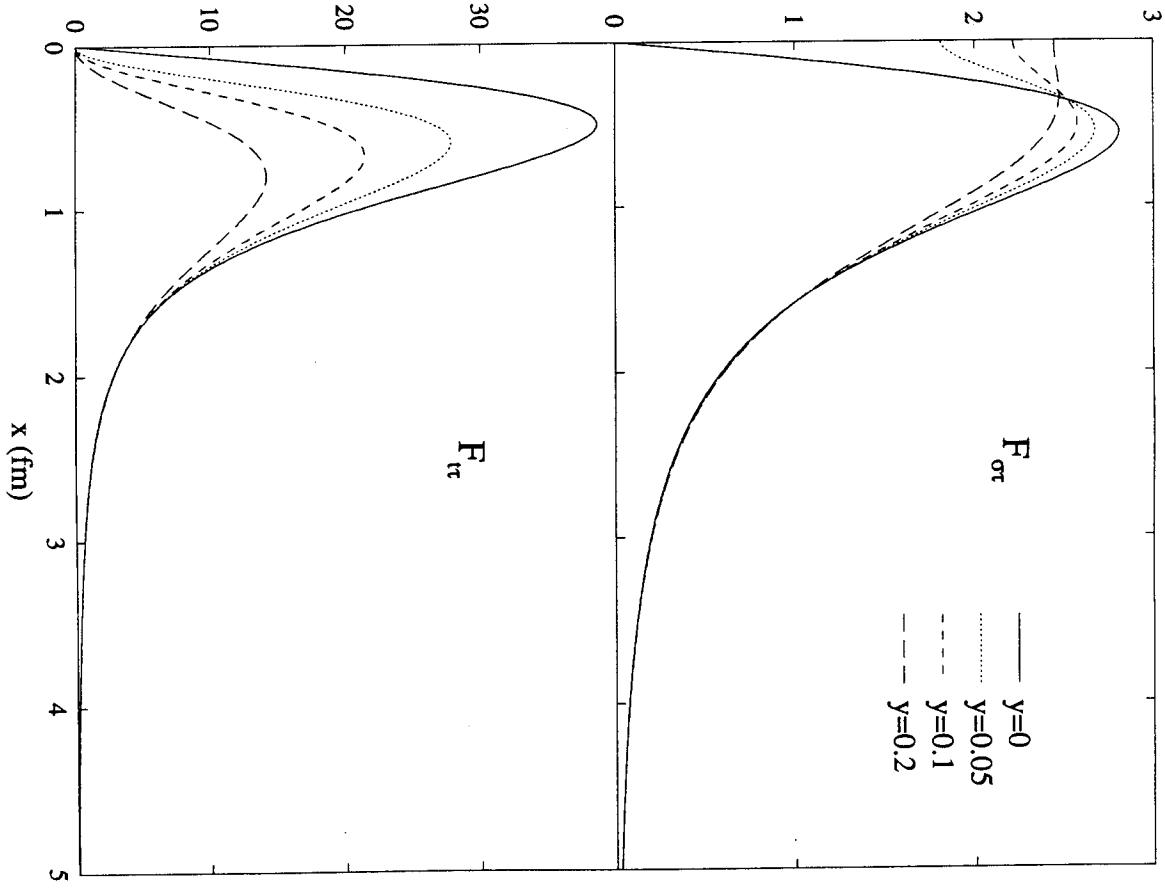
$F_{\tau\tau}$
$F_{\sigma\tau}$
x (fm)
y=0
y=0.05
y=0.1
y=0.2
0
10
20
30
1
2
3
4
5

Fig. 6

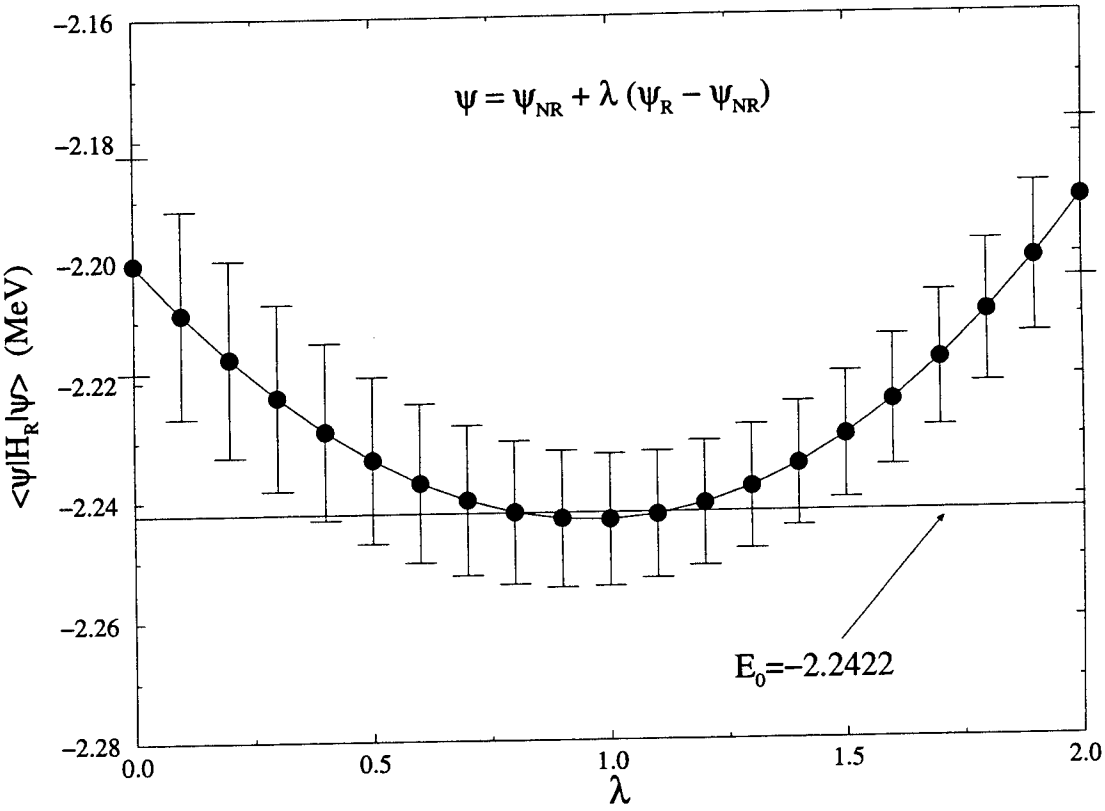
$\psi = \psi_{NR} + \lambda\,(\psi_R - \psi_{NR})$
$\langle\psi|H_R|\psi\rangle$ (MeV)
λ
E_0=−2.2422
−2.16
−2.18
−2.20
−2.22
−2.24
−2.26
−2.28
0.0
0.5
1.0
1.5
2.0

Fig. 7

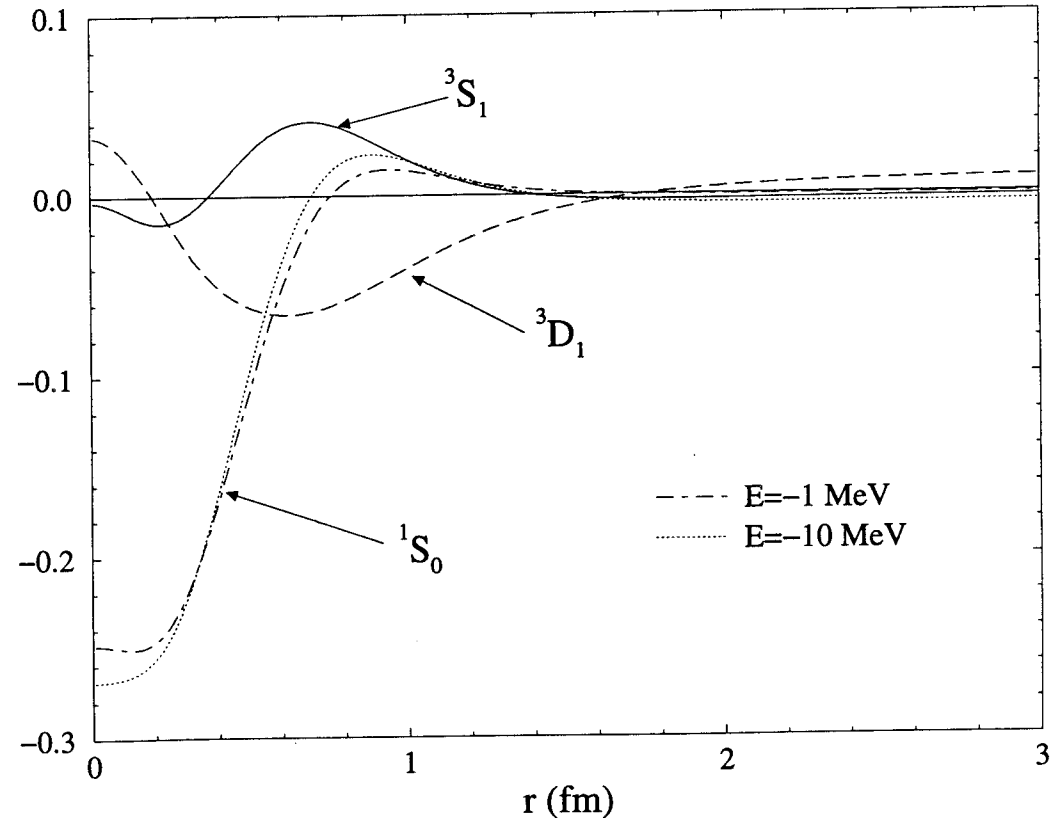
$^3S_1$
$^3D_1$
$^1S_0$
E=−1 MeV
E=−10 MeV
r (fm)
0.1
0.0
−0.1
−0.2
−0.3
0
1
2
3

Fig. 8

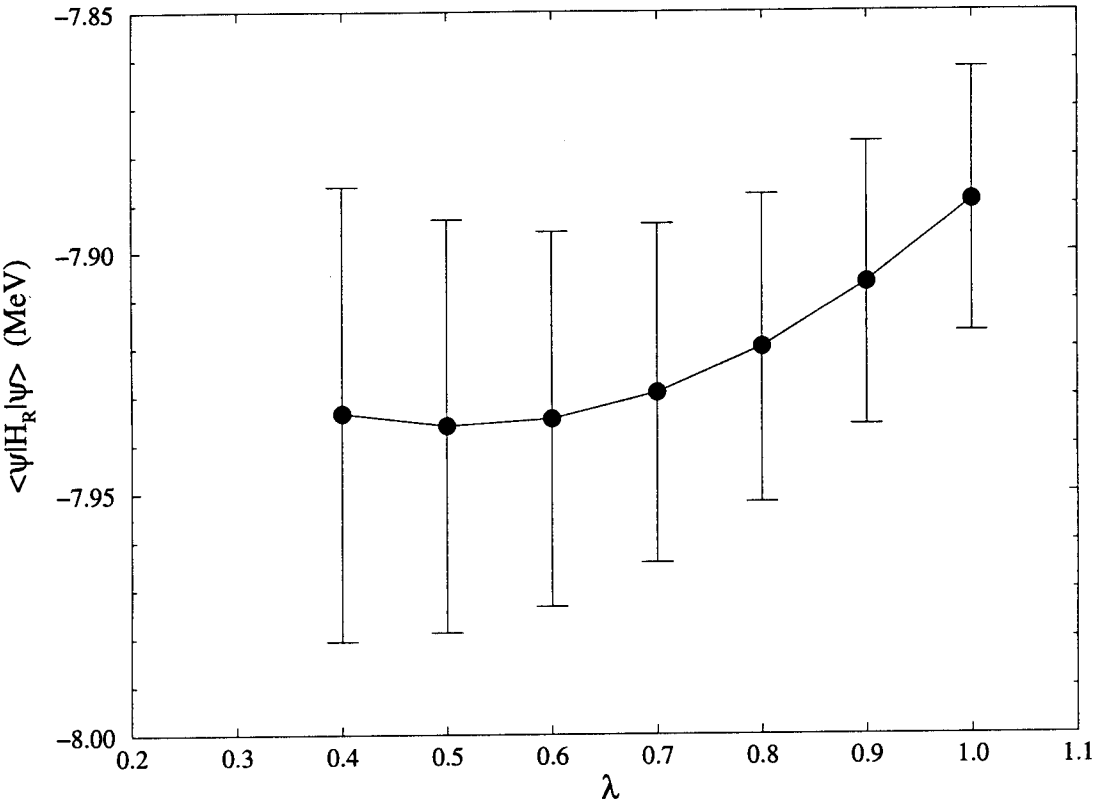
−7.85
−7.90
−7.95
−8.00
0.2
0.3
0.4
0.5
0.6
0.7
0.8
0.9
1.0
1.1
λ
<ψ|H_R|ψ> (MeV)

Fig. 9

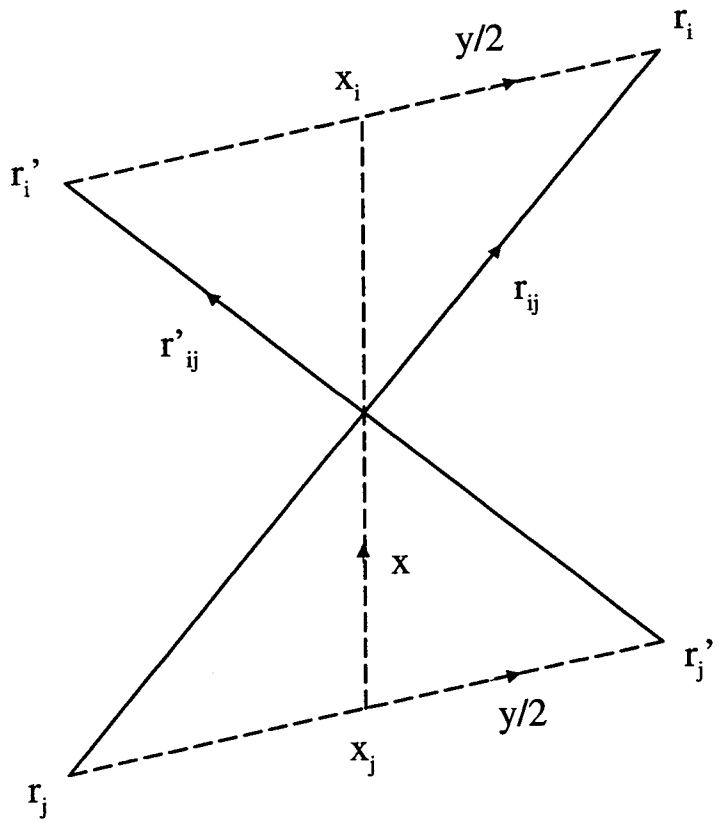
r_i
y/2
x_i
r_i'
r_ij
r'_ij
x
r_j'
y/2
x_j
r_j

Fig.

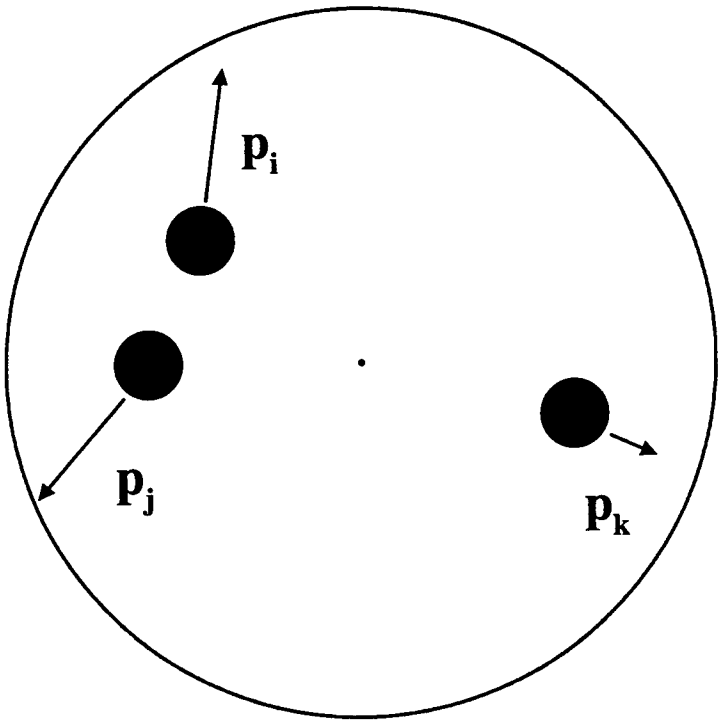

Fig 11